Internal features, mineralogy and geochemistry of ferromanganese nodules from the Gulf of Cadiz: The role of the Mediterranean Outflow Water undercurrent

F.J. González , L. Somoza , R. Lunar , J. Martínez-Frías , J.A. Martín Rubí , T. Torres , J.E. Ortiz , V. Díaz-del-Río

Geological Survey of Spain (IGME), C/ Ríos Rosas 23, 28003 Madrid, Spain
Departamento de Cristalografía y Mineralogía (UCM), C/ José Antonio Novais 2, 28040 Madrid, Spain
Centro de Astrobiología (CSIC/INTA), 29006 Torrejón de Ardoz, Madrid, Spain
Laboratorio de Estratigrafía Biomolecular (ETSIM/UPM), C/ Ríos Rosas 21, 28003 Madrid, Spain
Centro Oceanográfico de Málaga (IEO), Apdo. 285, 29640 Fuengirola, Málaga, Spain

A B S T R A C T

A large suite of Fe–Mn nodules (561 samples) were recovered during the *Anastasya 2001* cruise (TASYO project) along the continental margin of the Gulf of Cadiz (Eastern Central Atlantic), at the confluence of the Mediterranean Sea with the Atlantic Ocean, where extensive nodule fields were discovered. Based on wide previous studies that included swath bathymetry, multi-channel and very high-resolution seismic reflection, gravimetry, magnetism, heat flow probes and underwater photography surveys, nodules were collected at water depths ranging from 850 to 1000 m, associated with hydrocarbon-derived Mg-calcite, ankerite and dolomite chimneys and crusts. Forty-six selected samples among the various morphological types were used for the laboratory analysis of physical properties (morphology, color, surface texture, sphericity, weight and size), mineralogy (XRD, optical and electronic microscopy), geochemistry (XRF, AAS, ICP-MS, ICP-AES, EPMA, and GC-MS) and stable isotopes. The nodules show a wide range of sizes, densities, weights and morphologies. They are formed by multiple millimeter-thick layers of Fe and Mn oxyhydroxides surrounding the nucleus composed of Early–Middle Miocene plastic marl and sediment, which were derived from underlying units by fluid venting. Massive, laminated, detrital and mottled to dendritic textural features were developed by the Fe and Mn oxyhydroxide layers. The main components are Goethite, lepidocrocite, Mn oxides (7 Å manganates and 10 Å manganates), quartz, and phyllosilicates. Accessory minerals are calcite, dolomite, siderite, rhodochrosite, kutnahorite, pyrite, chalcopyrite, potassium feldspar, zircon, rutile, ilmenite and chlorite. Fe–Mn carbonates from the siderite–rhodochrosite continuous series are the principal constituent of the nuclei. Framboidal, filamentous and globular textures are observed in Fe–Mn oxides and pyrite, suggesting biogenic origin. The nodules show a high mean abundance of Fe (38.6%), moderate Mn (6.0%) and low contents of trace metals and REEs compared to the average content of deep-seabed polymetallic nodules from other oceanic areas. The Mn/Fe ratio ranges from 0.07 to 0.25. The studied nodules hold hydrocarbons (*n*-alkanes) derived from marine bacterial activity in their oxide layers, with the presence of aromatic hydrocarbons as phenanthrene as well, characteristic of mature petroleum. The structure, mineralogy and chemical composition in the studied nodules are more similar to those of diagenetic–hydrogenetic continental margin nodules rather than deep-sea nodules. We suggest that the formation of this type of nodule could respond to a combined diagenetic–hydrogenetic growth process, where the fluid venting from deep-seated hydrocarbon reservoirs, the bio-mineralization processes and the bottom currents erosion and chemistry could have played an important role.

1. Introduction

Since their discovery at the end of the nineteenth century (Murray and Renard, 1891), ferromanganese (Fe–Mn) concretions (nodules and crusts) have been explored and investigated in all the world ocean basins. Fe–Mn deposits occur in a wide variety of geological contexts (abyssal plains, spreading centers, and oceanic highs) and marine environments (deep oceans, continental margins, shallow waters, and

epicontinental seas) (e.g., Cronan, 1977; Glasby, 1977; Hein et al., 1997; Nicholson et al., 1997; Rona, 2003; Dekov and Savelli, 2004; Verlaan et al., 2005; González et al., 2007). Ferromanganese nodules and crusts have been classified according to their origin as hydrothermal, hydrogenetic and oxic or suboxic diagenetic, occurring in all these geological and oceanographic contexts (Bonatti et al., 1972; Dymond et al., 1984). Initially, polymetallic nodules were considered a potential economic resource of great interest because they contain strategic metallic elements (e.g. Cu, Ni, Co, Zn) (Rona, 2002). For the last few decades, research on Fe–Mn nodules and crusts has increased because of their utility in the study of paleoceanographic/paleoclimatic interactions (e.g., Koschinsky et al., 1996; Hein 2001; Claude et al., 2005). Usually, ferromanganese concretions have a low growth rate and they can record the physico-chemical conditions of the environment of deposition throughout time in their oxide layers (e.g., Eisenhauer et al., 1992; Hein et al., 1992; Abouchami et al., 1999). Therefore we can infer paleoceanographic and/or paleoenvironmental conditions in the deposit area through the study of the textural, mineralogical and geochemical characteristics of the ferromanganese concretions.

The Gulf of Cadiz is located at the South-Eastern sector of the North Atlantic Ocean (Fig. 1), between 34–37° N latitude and 5°30′–9°30′ W longitude. Towards the East, the Gulf of Cadiz is connected to the Mediterranean Sea by the Strait of Gibraltar, the place of interchange between the Atlantic and Mediterranean water masses. This location makes the Gulf of Cadiz unique because the interaction between the water masses with the continental margin could have played an important role in the depositional system throughout the most recent geological times (Hernández-Molina et al., 2006). Moreover, the Gulf of Cadiz represents a key area for deep thermohaline circulation and the global climate (O'Neill-Barringer and Price, 1999). In recent years the Gulf of Cadiz has been the focus of intensive research activity, with numerous oceanographic cruises carried out by multidisciplinary international groups (e.g., TASYO project, TTR-IOC UNESCO cruises, SONNE cruise and EuroCORE–EuroMARGINS projects). These efforts have contributed to the discovery and definition of one of the biggest mud volcanism provinces in Europe and have improved our understanding about this interesting area where complex links between oceanography, geology and biology exist. In this framework numerous

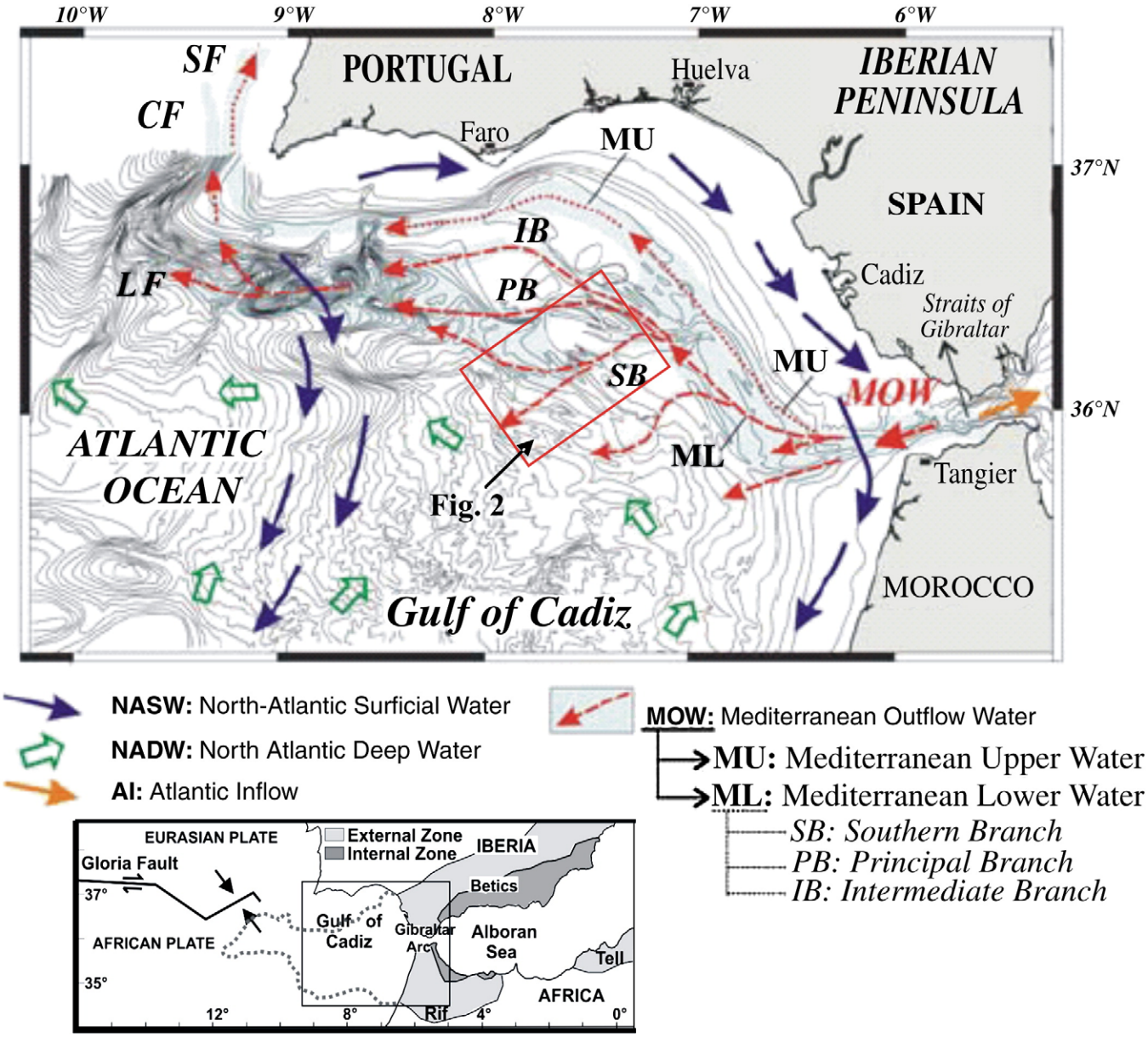

Fig. 1. Geological setting, water mass distribution and circulation and simplified bathymetry of the Gulf of Cadiz. The rectangle marks the situation of the nodule fields in the Guadalquivir Diapiric Ridge area (GDR). Bathymetry in meters. Partially modified from Hernández-Molina et al. (2003) and León et al. (2006).

fluid-escape structures and their associated deposits and ecosystems (e.g. mud volcanoes, extrusive deposits, pockmarks, gas hydrates, authigenic precipitates, chemosynthetic communities, cold-water corals) are being investigated in the Gulf of Cadiz (Ivanov et al., 2000; Gardner, 2001; Somoza et al., 2002, 2003; Díaz-del-Río et al., 2003; Magalhães et al., 2005; León et al., 2006).

Furthermore, contourite deposits linked to the action of the Mediterranean Outflow Water (MOW) and its relation to paleoceanographic/paleoclimatic events have been discovered in the area (e.g., Faugères et al., 1984; Hernández-Molina et al., 2003; Llave et al., 2006). Recently, Fe–Mn nodules have been described for the first time in carbonate-mud mounds related to fluid venting and strongly influenced by the MOW circulation (González et al., 2007).

This paper presents a detailed structural, textural, mineralogical, and geochemical description of the Fe–Mn nodules that were recently discovered along the continental margin of the Gulf of Cadiz. We propose that the nodules are associated with hydrocarbon-related seeps and strongly influenced by the MOW undercurrent circulation. In addition, we present a comparative analysis with other deep-seabed polymetallic nodules, and shallow-water and continental margin nodules from other ocean basins and tectonic settings around the world.

2. Oceanographic and geological framework

The Gulf of Cadiz is connected to the Mediterranean Sea by the Strait of Gibraltar where the Atlantic and Mediterranean water masses meet (Ochoa and Bray, 1991). From the Late Pliocene (2.4 Ma) to the present day, the circulation pattern in the Gibraltar gateway has been characterized by the outflow of warm and saline Mediterranean waters (MOW) near the bottom, and the inflow of less saline and cool Atlantic waters (NASW) on the surface (Loubere, 1987; Nelson and Maldonado, 1999; Hernández-Molina et al., 2006). MOW is a strong current that circulates across the slope of the Gulf of Cadiz from the SE to the NW (Ochoa and Bray, 1991; Hernández-Molina et al., 2003). MOW divides into two main cores: Mediterranean upper and lower waters, moving across the upper slope (500–800 m) and the middle slope (800–1200 m), respectively (e.g., Ambar and Howe, 1979a,b; Gardner and Kidd, 1987; Hernández-Molina et al., 2006; Llave et al., 2006). The North Atlantic Deep Water (NADW) is situated below the MOW (Ochoa and Bray, 1991). The MOW circulation is affected by the bottom topography, giving rise to different sedimentary features (e.g., channels, contourite deposits, ripples, dunes). All of these depositional systems have been influenced in the Late Quaternary by climatic and sea-level changes, oceanographic conditions and local tectonic events (Hernández-Molina et al., 2006). Therefore the MOW circulation is strongly conditioned by seabed morphology and it controls the morphology and near-surface deposits because of their strong erosive action. Moreover, the specific physical–chemical characteristics of the MOW can be reflected in the deposits generated, as occurs in Fe–Mn nodules and carbonate chimneys (González et al., 2007), which are very useful in inferring paleoceanographic/paleoclimatic changes in the past. During the Late Quaternary, the sedimentary model of the Gulf of Cadiz is different in the cold stages and the warm stages, the MOW circulation being a principal actor at this time. During the cold events, the middle slope is strongly influenced by the MOW action in its lower core, whereas in the warm periods the upper core of the MOW is the most active (Llave et al., 2006; Hernández-Molina et al., 2006).

The Gulf of Cadiz is located at the westward front of the Betic–Rifean Arc, in the easternmost sector of the Azores–Gibraltar segment of the Africa/Eurasia collisional plate boundary (Dewey et al., 1989) (Fig. 1). The Gulf of Cadiz represents one of the biggest mud volcanic provinces in Europe, where the combined influence of the NADW and the MOW water masses can play an important role over the geological and microbiological processes at the seafloor. The morphology of the middle slope is characterized by a terrace configuration ("slope terrace"), related to the progressive emplacement of an allocthonous wedge since the Middle-Miocene in the eastern and central parts of the margin, and the construction of the Betic–Rifean external front (Medialdea et al., 2004). The study area is situated in the NE sector of the middle slope of the Gulf of Cadiz, at a depth of 900–1000 m, where the lower core of the MOW is moving and giving rise to different morphologies and seabed deposits (Fig. 2). This region is characterized by NE–SW trends of

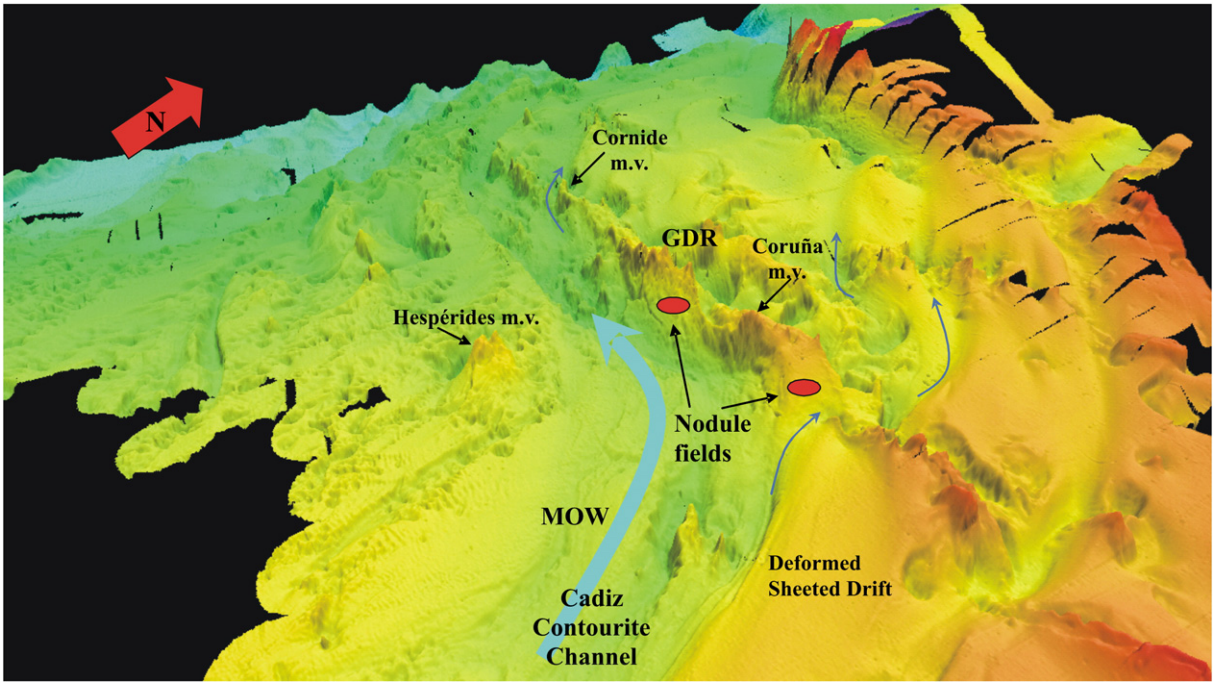

Fig. 2. 3D multi-beam bathymetric image (Simrad EM12-120S), *Fledermaus* visualization of the seabed structure map in the studied area. Viewing direction is from the East. Cool colors indicate deep water, warm colors indicate shallow water. Vertical scale enlargement is 2×. For scale and location see Fig. 1. The NNE–SSW alignments of mounds and mud volcanoes (Coruña and Cornide) from the Guadalquivir Diapiric Ridge (GDR) suppose a barrier to the lower core of the MOW giving rise to the Cadiz Contourite Channel and contouritic drifts. Red ovoids represent the location of the main ferromanganese nodule fields. Blue arrows indicate the MOW undercurrent direction in this sector.

diapiric structures as the *Guadalquivir Diapiric Ridge* (GDR) and channels as the *Cadiz Channel* (CC) where the MOW circulates (Fig. 2) (Somoza et al., 2003). Diapir ridge formations are related to the complex tectono-sedimentary history of this area, where a combination of gravitational, tectonic and sedimentary processes is configuring the actual geological framework. GDR is located at the "*Cadiz Allocthonous Unit*", a chaotic and highly diffractive body composed of a mixture of Triassic, Cretaceous, Paleogene and Neogene sedimentary units, overlaying a Paleozoic basement (Maldonado et al., 1999, Medialdea et al., 2004). It involves a huge volume of mud and salt diapirism associated with Triassic salt units and Early–Middle Miocene plastic marls (Maldonado et al., 1999). Throughout this area, extensive hydrocarbon-rich fluid venting and mud diapirism are observed, which include numerous mud volcanoes, methane-related authigenic carbonates (crusts, chimneys and carbonate mounds) and pockmarks (Baraza and Ercilla, 1996; Gardner, 2001; Ivanov et al., 2000; Díaz-del-Río et al., 2003; Pinheiro et al., 2003; Somoza et al., 2003). These are related to the lateral compression from the Africa–Eurasia convergence, which promoted fluid migration to the surface. GDR presents numerous highs, lows and gaps, and exhibits evidences of extrusive activity and mud volcanism from the Middle-Miocene to the present (Fernández Puga, 2004; León et al., 2007). The channels (e.g., CC), due to the strong erosive action of the bottom currents combined with tectonic activity, are characterized in their floor by very high backscatter representing outcrops of diapirs and rocks (Hernández-Molina et al., 2006). The CC, where the MOW is circulating in the study area, is the largest and most important contourite channel in this sector. It has a length of 110 km and variable depth (up to 120 m) and direction, being NE–SW and sub-parallel to the ridge in the GRD sector (Hernández-Molina et al., 2006). In this sense, the GDR forms a topographic high that constricts the MOW circulation pathways, dividing the current into minor branches (Nelson et al., 1993; Hernández-Molina et al., 2003).

3. Materials and methods

The Gulf of Cadiz area has been extensively surveyed previously with swath bathymetry, multi-channel and very high-resolution seismic reflection, gravimetry, magnetism, heat flow probes, underwater cameras, dredging, and gravity coring (Baraza and Ercilla, 1996; Gardner, 2001; Díaz-del-Río et al., 2003; Pinheiro et al., 2003; Somoza et al., 2003; Medialdea et al., 2004; León et al., 2007).

3.1. Field site and sample suite

Samples of ferromanganese nodules, carbonate chimneys and crusts, and host sediments (mud-breccia) were collected from the GDR area, located on the northeast middle slope of the Gulf of Cadiz (Eastern Central Atlantic Ocean). Nodules were recovered during cruise *Anastasya 2001* aboard the research vessel "*Cornide de Saavedra*" using rectangular benthic dredges. Previously collected dredges, bottom photograph surveys and sediment cores indicate the presence of Fe–Mn nodules within the area of high backscatter. The samples recovered comprise 561 ferromanganese nodules with a total weight of 36.6 kg. Nodule fields extend in a region along the middle continental slope at an average depth of 900 m (González et al., 2006a).

The study of 46 selected samples between distinct nodule types was carried out in the "Centro de Astrobiología" (CAB/CSIC), "Centro de Microscopía Electrónica y Citometría" at the Complutense University of Madrid (UCM), the "Laboratorios del Instituto Geológico y Minero de España" (IGME), the "Laboratorio de Isótopos Estables" at the University of Salamanca (USAL), and the "Laboratorio de Estratigrafía Biomolecular" at the Polytechnic University of Madrid (UPM). The selection of samples was based on their superficial color, external morphology and size. Selected samples were cut vertically in two halves with respect to their position on the seafloor before macroscopic internal descriptions and physical, XRD, petrographical or chemical analysis. Individual layers of special interest for geochemical and mineralogical determinations were sampled under the microscope with a needle drill.

3.2. Physical properties and surface texture characterization

For weight and maximum diameter measurements, and color and superficial texture characterization, all the nodules collected were used. Apparent wet bulk density and open porosity were determined by water absorption in void according to the UNE-EN 1936:1999 normative. Real dry bulk density was calculated by the helium pycnometer method with an Accupyc 1330 pycnometer. Color was determined by comparison with the Munsell color charts (Munsell Color Co., 1980).

3.3. Mineralogy

Petrographical and XRD studies reflect the mineralogical composition of the studied nodules and their microtextural features. The samples were first thoroughly examined by transmitted and reflected light microscopy, and the internal structure was described, outlined and photographed. In all, 29 polished sections, 24 thin sections and 46 polished specimens were examined. Bulk mineralogical X-ray diffraction (XRD) profiles from $2\theta = 2–60°$ in 0.005 steps were obtained in 25 samples using XPERT PRO of PANalytical, Cu-Kα radiation (35 kV and 40 mA) with graphite monochromater, software *High Score* and ICDD data base. Scanning electron microscopy (SEM-EDS) of morphological and 3D textural mineral characteristics was performed on a JEOL JM-6400 instrument.

3.4. Geochemistry

Bulk nodules and selected layers and minerals were prepared and analyzed in order to define their chemical composition. Thirty-six bulk nodules were measured for major (Al, Fe, Mn, Ca, Mg, Si, K, Ti and P) and trace elements (Sc, V, Cr, Co, Ni, Cu, Zn, Pb, Sr, Ba, Br, Rb, Zr, Th, U, As and Mo) by X-ray fluorescence (XRF) using a MagiX of PANalytical instrument with Rh radiation. Au, Na and Li were measured using atomic absorption with a VARIAN FS-220 and B by induced coupled plasma atomic emission spectrometry (ICP-AES). Accuracy of the data was checked by using international standard reference materials, and precision based on duplicate samples was found to be better than $\pm 5\%$. Loss on ignition (LOI) was determined by calcination at 950 °C and S was measured in ELTRA CS-800 equipment. The bulk REE concentrations of selected samples were determined by induced coupled plasma mass spectrometry (ICP-MS-TOF) in a RENAISSANCE instrument. The standard reference materials SO-1 (CCMET), GSP-1 (USGS) and BCR-1 (USGS) were used to test the analytical procedure for REE determinations. The accuracy and precision obtained were better than 10% for all REE. TOC was made for 14 bulk nodules by subtracting the TIC obtained by calcination at 550 °C from the TC values and measured in ELTRA CS-800 equipment. Multielemental spot analyses and mapping profiles, in mineral phases and textural features, were carried out in the interesting areas determined by petrographic studies using electron probe micro analysis (EPMA) with a JEOL Superprobe JXA-8900 M, operating at 15–20 kV and 50 mA, fitted with wavelength dispersive spectrometers (WDS). Back-scattered electron images were also obtained with this instrument. Standards included pure metals, synthetic and natural minerals, all from international suppliers. Biomarkers were analyzed by combined gas chromatography–mass spectrometry (GC–MS). Component identification was based on comparison of the mass spectra and the GC retention times with published data and reference compounds.

3.5. Stable isotopes

Carbon and oxygen isotopic signatures were measured in carbonate rhomboidal crystals extracted from the nucleus of the

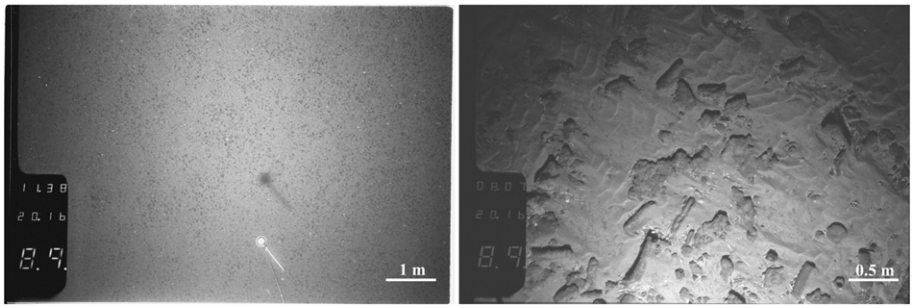

Fig. 3. Underwater images showing Fe–Mn nodules, in the left photograph, and carbonate chimneys and crusts, on the right, lying on the seabed. They were photographed in the surroundings of the Guadalquivir Diapiric Ridge area (with a rectangle in Fig. 1). The nodules in patchy distribution are close to hydrocarbon-derived carbonate slabs covered by cold-water corals, sponges, and echinoids. The sedimentary structures show well developed asymmetrical ripples due to the undercurrent action.

nodules. Sulphur isotopes were calculated in pyrites obtained from the Fe–Mn layers. Carbon and oxygen isotope measurements were carried out by fractionated extraction of carbon dioxide (Walters et al., 1972; Al-Aasm et al, 1990) with 103% phosphoric acid at 25 °C/2 h for calcite, 25 °C/2 days for dolomite, 25 °C/2 days for rhodochrosite and 50 °C/9 days for siderite. Isotopic ratios were measured in a SIRAII VG-Isotech mass spectrometer. For sulphur isotope analyses SO_2 was extracted from pyrite by void combustion in presence of Cu_2O according to the methodologies of Robinson and Kusakabe (1975) and Coleman and Moore (1978), and measured in a SIRAII VG-Isotech mass spectrometer. The reproducibility of the analytical procedure was better than 0.2‰ for sulphur, carbon and oxygen.

3.6. Statistical analyses

The inter-element associations were determined using SPSS-13 software, and only the significant associations ($r \geq 0.35$ at 95% and 99% confidence levels) were used.

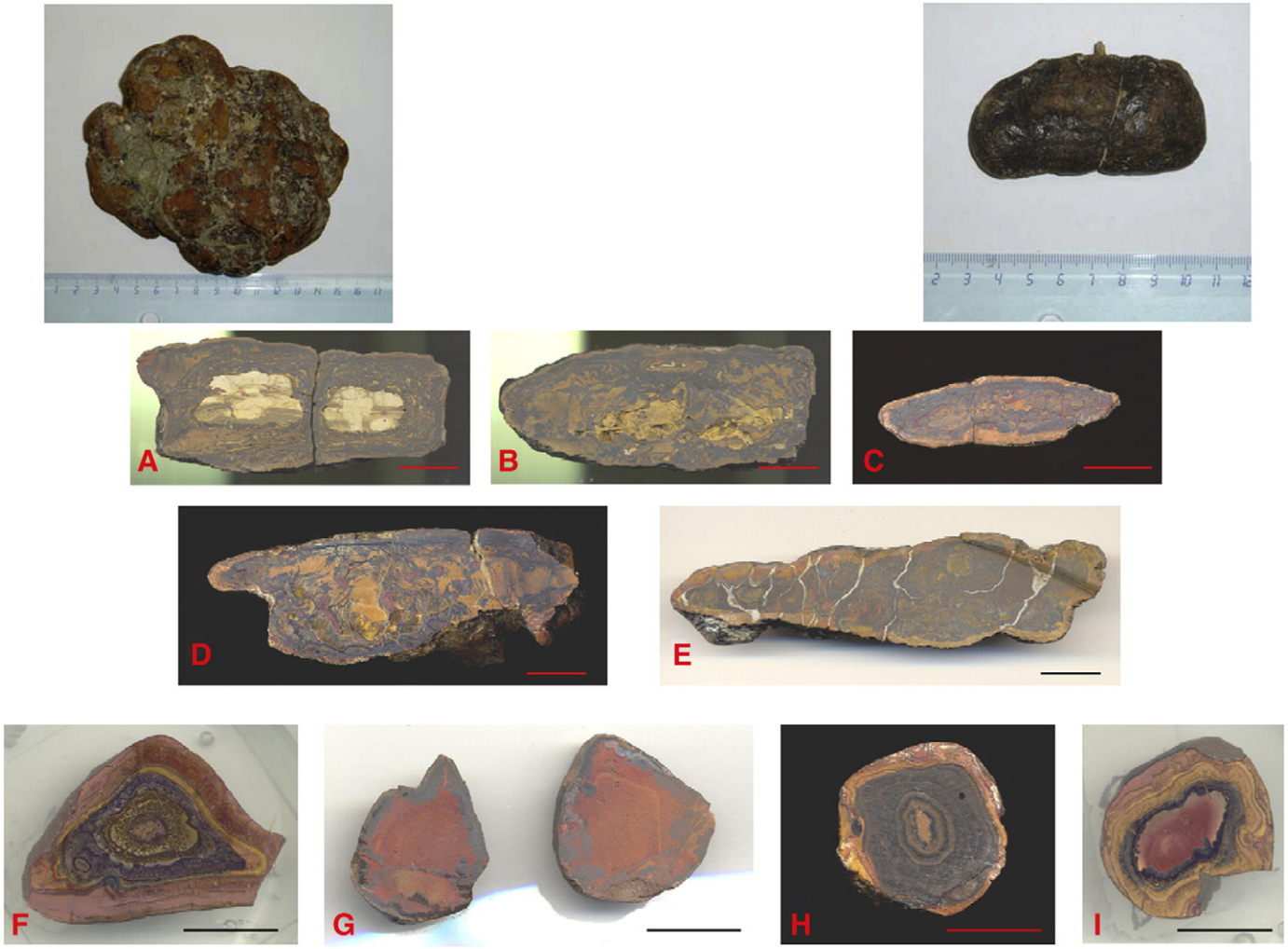

Fig. 4. Sections of different morphological types of nodules, showing the most typical macroscopic internal features. Tabular to irregular big nodules are shown in images A, B, C, D and E. The photographs F, G, H and I show sub-spherical to spherical small nodules. The external layers are affected by alteration front discontinuity, especially visible in the pictures H and I. In the E section we can observe different fractures crosscutting the nodule that are filled with detrital sediments and mineral precipitates. Scale bar represents 1 cm. The top two pictures of Fe–Mn nodules show smooth (on the right) and rough (on the left) surface texture.

Table 1
General physical characteristics of the nodules from the Gulf of Cadiz.

Maximum diameter (cm)	1.6–20.4
Dry weight in air (g)	1.37–1818.8
Apparent wet bulk density (g/cm^3)	1.8–2.6
Real dry bulk density (g/cm^3)	3.3–3.5
Open porosity (volume %)	23.9–44.3
Color	Orange–black

4. Results

4.1. Nodule occurrence and external features

On the *Anastasya 2001* cruise several ferromanganese nodule fields were discovered at the base and flanks of the GDR at the NE sector of the Gulf of Cadiz (González et al., 2007), which is characterized by abundant carbonate chimneys and crusts on top of the ridge (Díaz-del-Río et al., 2001; Somoza et al., 2003; Fernández Puga, 2004). A number of individual carbonate-mud mounds were identified along the GDR (Fig. 2). This ridge is surrounded by channels as the Cadiz Channel, on the south side, through which the MOW undercurrent circulates and protrudes an intensive erosive action, configuring a contourite depositional system (Hernández-Molina et al., 2006). Dredge hauls from the top of these mounds yielded large amounts of carbonate crusts and chimneys and mud-breccia flow deposits composed mainly of ejected materials, mostly Miocene marls and mud. Indications of gas saturation include degassing structures, the presence of hydrogen sulphide (H_2S), and chemosynthetic fauna (*Pogonophora* sp. tube worms, *Calyptogena* sp. and *Acharax* sp.) (León et al., 2007). The fields of ferromanganese nodules occur in a variable density overlying the seafloor at the base of the mounds, where the influence of the MOW is strong and where rippled seabed and carbonate crusts and chimneys also occur (González et al., 2006a) (Fig. 3).

Nodules are characterized by different morphological types: tabular, irregular, discoidal, sub-spherical, ellipsoidal, and cylindrical, but the most abundant is tabular morphology (Fig. 4). Tabular to irregular samples represent more than 90% of the nodules recovered. The surface texture is smooth to rough and botryoidal (Fig. 4). Edges of nodules are normally rounded. Superficial carbonate encrustations of tube worms and bryozoans are common and small cold-water corals are rarely present. Regarding carbonate chimneys and crusts, nodules do not present superficial boring by benthic organisms. Surface color varies between light orange and black, is independent of the size or shape of the nodule, and reflects the fundamental chemical composition of the external part of the samples: Fe oxyhydroxides (orange to red color) and Mn oxides (black color). Fractures with different directions, less than 1 cm in width and variable length, are visible on the surface, especially in big nodules. These fractures can be open or filled with bottom sediment and mineral precipitates. Table 1 shows the maximum diameter, weight, porosity, and dry bulk density of the nodules collected.

4.2. Internal structure

As shown by the photographs in megascopic polished sections in hand samples, we can distinguish three different structural elements in the nodules studied in this work: nucleus, layers and discontinuities.

Nodule growth always starts at a nucleus ranging in size from 1 mm to 4.5 cm. There are samples with one or several cores (polinucleated) (Fig. 4) and samples composed of the accretion of several nodules (polinodules). Two extreme kinds of nucleus in relation to their nature exist: nucleus composed of soft sediment with diffuse limits and nucleus composed of hard marl clasts with tabular morphology and well defined angular exterior edges. Both types of cores generally are impregnated by Fe–Mn oxyhydroxides, especially the nucleus composed of soft sediment. Nucleus color is beige, and it is orange to red when impregnated by oxides. The exterior shape of the nodule frequently reflects the shape of the nucleus. The small nodules, less than 2 cm in maximum diameter, have very small cores and result in spherical to sub-spherical nodules. Big samples normally have a large nucleus, commonly tabular, and result in tabular to irregular nodules.

The layers show dark colors or even opaque colors between yellow and black. The periodic growth of the nodules can be reflected by a well expressed concentric fabric, especially in small samples, which frequently present a succession of black layers (in which Mn oxides predominate) and yellow or brown ones (fundamentally with Fe-oxides). Nodules <2 cm in diameter have symmetric distribution of

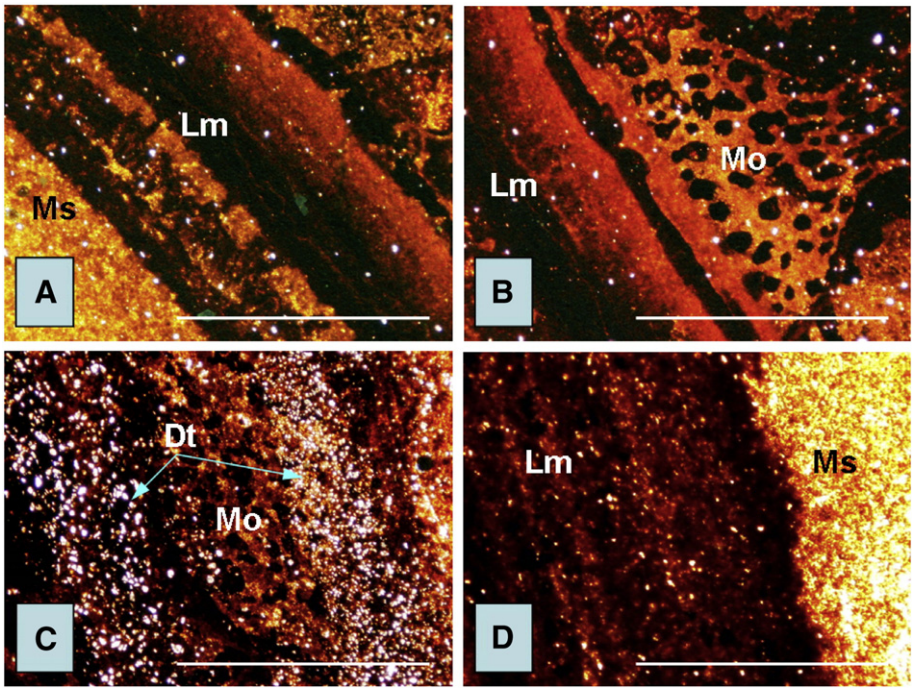

Fig. 5. Photomicrographs in transmitted polarized light. Four of the most characteristic structures of the studied nodules are observed: laminate (Lm), massive (Ms), detrital (Dt) and mottled (Mo). Scale bar represents 1 mm.

growth layers around the nucleus, but in larger samples the asymmetric and complex growth pattern is usual. Four different types of internal growth structure are identified: laminated, massive, mottled to dendritic, and detrital (Fig. 5).

Discontinuities disturb the normal development of growth layers. They are classified in five types: fracture discontinuities, growth discontinuities, burrowing discontinuities, fluidification discontinuities (probably related to fluid migration) and discontinuities of alteration (which affect 2–5 mm of exterior layers) (Fig. 4).

4.3. Mineralogy

The main components of the nodules are: goethite, lepidocrocite, 7 Å manganates, 10 Å manganates, pyrolusite, quartz and phyllosilicates (illite, smectite and kaolinite). Accessory minerals accompanying these major phases include calcite, dolomite, siderite, rhodochrosite, kutnahorite, pyrite, marcasite, chalcopyrite, potassium feldspar, zircon, rutile, ilmenite, apatite and chlorite. Gypsum is present as a trace secondary mineral. Fe–Mn oxides and oxyhydroxides represent a mean value of 75 wt.% of the nodular mass and they form an essential part of the layers. Nuclei are composed of carbonates (fundamentally siderite to rhodochrosite), silicates in minor proportion and disseminated pyrite as an accessory mineral. Silicates (especially in detrital layers) and carbonates dispersed in the oxide layers and concentrated within the nuclei represent about 25 wt.% of the nodular mass.

The SEM and EPMA images show a typical interlamination of Fe-rich layers (grey reflectivity) and Mn-rich layers (light grey to white), especially in small nodules. These layers form a micro-crystalline mosaic of rhombic crystal sections closely inter-grown in a cryptocrystalline matrix where detrital grains and framboids are dispersed in a variable degree of abundance (Fig. 6). These rhombic crystals are between 2 and 10 μm in size and normally present internal zoning with goethite concentrated on the external edge, and the nucleus of these crystals is formed by a mixture of goethite and Mn oxides. Matrix components are formed by a mixture of phylosilicates, Mn oxides, and carbonates (frequently filling micro-fractures). Detrital grains, mainly silicates, appear in two different ways: disperse in the matrix, or forming continuous layers very rich in detritals (detrital structure) and poor in Fe–Mn oxides. Goethite forming framboidal and sub-idiomorphic cubic/octahedral aggregates derived from partial or total replacement of pyrite and substituting carbonates of the bioclastic shells (bivalves, gastropods, ostracoda, foraminifera and other benthic organisms) are also observed. The external part of the nodules, affected by the discontinuity defined as alteration front, displays a colloform structure overprinted on the typical rhombic mosaic.

The nucleus displays the same micro-crystalline mosaic of rhombic crystal as the ferromanganese layers, but the rhombohedral crystals are formed by a zoned carbonate between siderite and rhodochrosite (mean of 37.6% FeO and 8.6% MnO; $n = 7$) in a matrix of phyllosilicates with dispersal detrital grains (essentially quartz and feldspar) and pyrite.

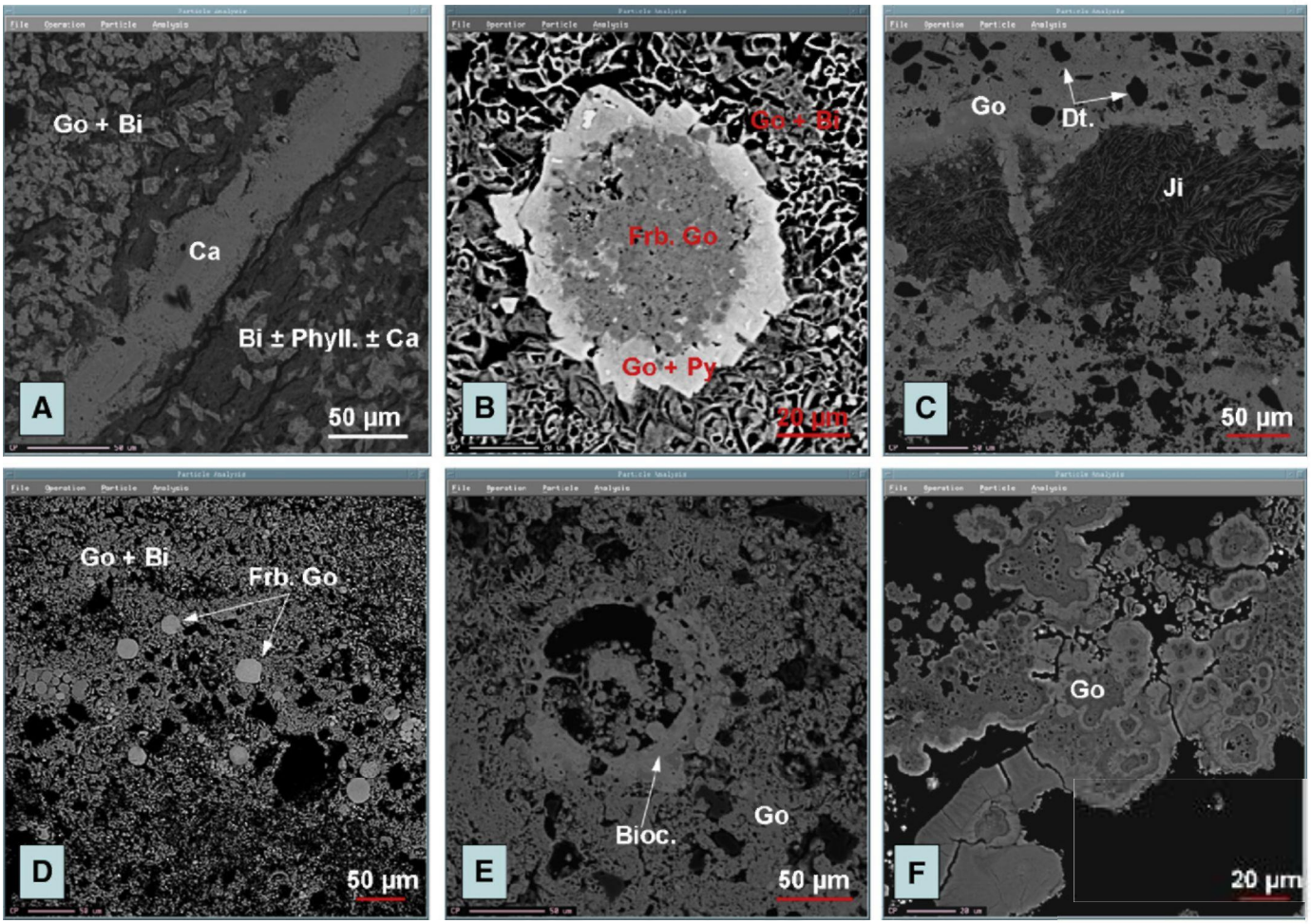

Fig. 6. Mineralogy and internal microtextures of the nodules, photomicrographs (back-scattered electrons). (A) Oxide layer showing goethite–birnessite rhombic crystals (Go + Bi) surrounded by Mn oxides (Bi) and crosscut by a post-accretional crack filled with carbonates (Ca). (B) Pyrite aggregate formed by framboids (inside) and idiomorphic cubic crystals (outside), partially pseudomorphised by goethite which is paragenetic with Fe–Mn rhombic crystals (Go + Bi). (C) Jianshuite (Ji) in feather structure filling up a void next to microcrystalline goethite (Go) with scattered detrital grains. (D and E) Framboidal goethite (Frb. Go) disperse or forming aggregates. This goethite is pseudomorphising previous pyrite and bioclast (Bioc.). (F) Colloform goethite filling a post-depositional crack.

SEM observations have revealed abundant structure-like microbes and filamentous morphology (length between 1–3 μm), composed of goethite with a significant quantity of C (up to 24%). Fibrous texture-like microbes coated by Mn oxides and rich in organic carbon have been identified in the pores of some samples (Fig. 7).

4.4. Chemical composition

4.4.1. Bulk sample geochemistry

Fe is the most abundant element in the nodules followed by Mn, Si and Ca. Major, trace and REE element abundances and ratios are presented in Table 2. The bulk chemical composition of Fe–Mn nodules in the Gulf of Cadiz varies from 0.07 to 0.25 for Mn/Fe ratio. Combined Cu + Ni + Co concentrations are very low, ranging from 0.01% to 0.05% with an average of 0.02%, very poor in respect to the mean values for oceanic nodules (0.14%) (Baturin, 1988). Si/Al ratio is between 1.91 and 3.46, with a mean of 2.52, generally below 3 (which is the marine sediment ratio) suggesting the presence of an important quantity of clay minerals into the nodules, as the bulk XRD analyses confirm. The highest standard deviations (61–138) are found in Ni, As, Sr, V and Ba contents. In relation to average crustal abundance (Evans, 1980), several elements are enriched in the nodules from the Gulf of Cadiz by different order factors: As (88), Mn (63), Mo (31), Fe (8), Co (4), V (2) and P (2). Al, Si, K and Na are depleted elements in respect to the crustal mean composition by a factor of between 6 and 11 (Fig. 8). Fe, Mn, Mo, Co, Ni, As and V are enriched in nodules in respect to the mud-breccia associated sediments. Nodules have similar enrichment in elements as Mn, Fe, Co or Ni, regardless of their size. Only Ca shows a relative positive correlation with the sample size, and large nodules are more enriched in Ca than smaller nodules.

Bulk average contents in REE in Fe–Mn nodules (78 μg/g) are lower than in mud-breccia associated sediment (171 μg/g). Shale-normalized REE generally shows a zero to slightly negative Ce anomaly ranging between −0.11 and +0.04, and positive Eu anomalies (Fig. 9). Therefore their REE concentrations can be explained by the significant terrigenous components and by the enrichment of REE in Fe–Mn oxide precipitates.

In bulk sample (Table 3), Fe displays positive correlation with P ($r = 0.41$, $n = 35$) and Cu ($r = 0.41$, $n = 34$), and negative correlation with Mn ($r = -0.56$, $n = 35$) and S ($r = -0.51$, $n = 24$). Mn has strong negative correlation with P ($r = -0.70$, $n = 35$), Co ($r = -0.64$, $n = 34$), Zn ($r = -0.53$, $n = 34$) and positive with Ba ($r = 0.62$, $n = 34$), Sr ($r = 0.42$, $n = 34$) and Na ($r = 0.36$, $n = 35$). Ca is correlated with Mg ($r = 0.53$, $n = 35$) and P ($r = 0.50$, $n = 35$). High correlation exists between Si, Al, Ti and K. Th and U concentrations present positive correlation ($r = 0.48$, $n = 34$).

4.4.2. Distribution of elements in the nodule

The geochemical characteristics of each nodule usually vary from the outer part to the core and from one concentric layer to another. The Mn and Fe concentration curves in EPMA profiles have an irregular shape with different peaks of maximum contents of these metals. The concentric growth pattern of alternating Fe and Mn generally shows Mn concentrated close to the nucleus of the nodule, decreasing its concentration towards the periphery (Fig. 10). The Fe components show an opposite trend and they are more concentrated towards the exterior of the nodule. Nuclei are enriched in Ca and Mg related with carbonates, and terrigenous elements (Si, Al) linked to the scattered silicate minerals.

As shown by EPMA analyses (maps and profiles), one group of elements (Fe, P, Zn, V, As and Co) concentrates more on the external edge of the nodules affected by the alteration front (Figs. 10 and 11). These layers are depleted in Mn. For most of the trace elements any preferable accumulation trend is observed in the nodules. In general Fe and Mn oxides are dominant in the layered structure and therefore the elements associated with their mineral phases are predominant. Fe oxyhydroxides (mainly goethite) concentrate the largest contents in Fe and important quantities of Si, Al and Ca, and minor of S, Co and P, and appear concentrated in the laminated structure. Goethites derived from pyrite replacements (e.g., cubic crystals and framboids)

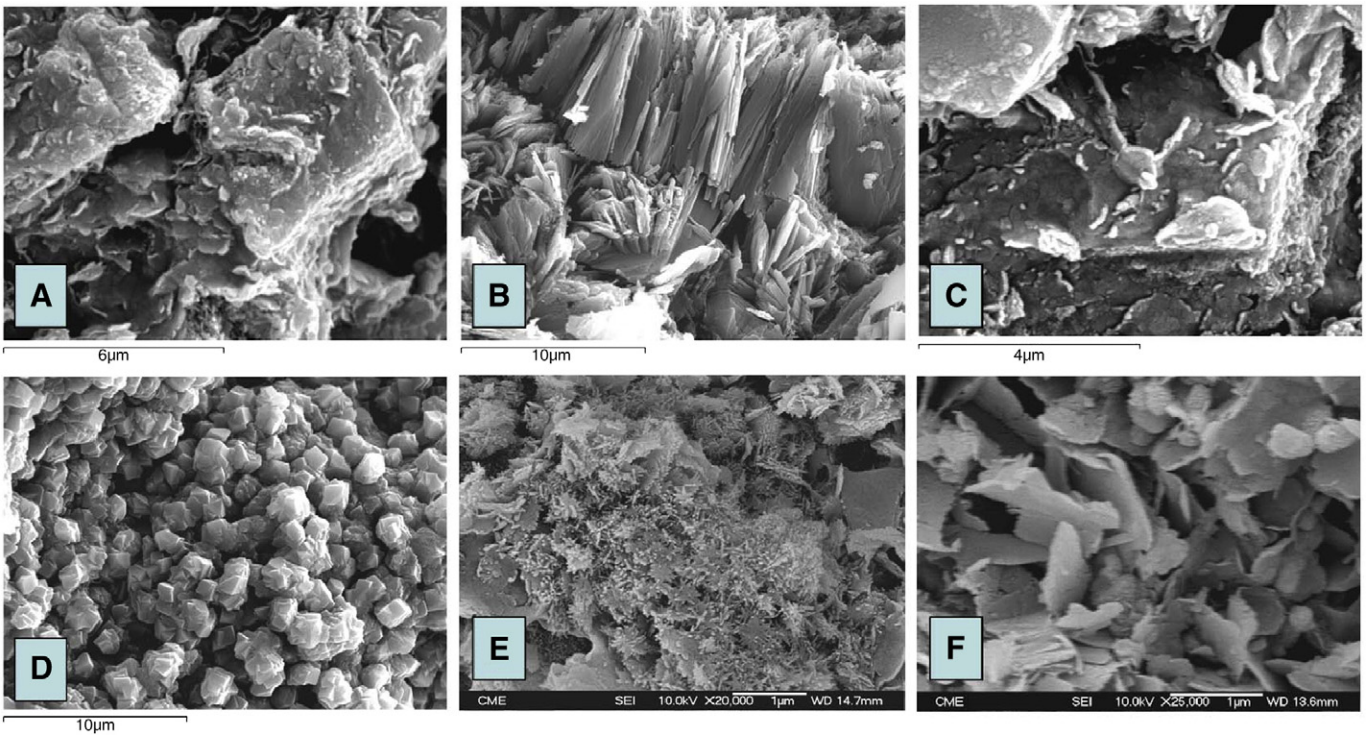

Fig. 7. 3D scanning electron microscope (SEM) micrographs of textural features from the nodular mineralogical components. (A) Rhombohedra crystal of Fe-dolomite pseudomorphised by Fe–Mn oxides. (B) Platy goethite filling micro-fractures. (C) Rod-shaped bacteria-like texture (arrows) coated with a fine grained Fe–Mn oxide precipitate. (D) Pyrite aggregate composed by multiple cubic micro-crystals partially transformed into Fe-oxides. (E) Growth of Fe-oxides in flower shape within the oxide layers. (F) Tabular crystals of Fe–Mn oxides.

Table 2
Average content and ratios of major (wt.%), traces and REE elements (μg/g) of the nodules of the Gulf of Cadiz, one sample of the mud-breccia host sediments and shallow-water nodules from the Black Sea (data from Sevastýanov and Volkov (1967), Fomina and Volkov (1969) and Bogdanov et al. (1995)).

Element	Max	Min	Mean	No. of samples analyzed	Mud-breccia host sediment	Black Sea shallow-water nodules
(%)						
Al	1.98	0.92	1.38	36	6.24	1.65
Si	5.26	1.75	3.48	36	22.08	5.56
P	0.30	0.05	0.19	36	0.53	1.14
K	0.64	0.20	0.34	36	1.56	–
Na	0.69	0.03	0.26	36	0.11	–
Ca	6.57	0.62	3.15	36	9.82	4.45
Mg	2.21	1.03	1.83	36	1.61	1.04
Ti	0.14	0.06	0.10	36	0.37	0.1
Fe	45.06	33.06	38.58	36	3.47	26.54
Mn	9.12	3.01	6.03	36	0.03	6.79
S	0.47	0.05	0.12	24	0.45	–
LOI	23.24	13.86	18.05	24	15.63	–
Mn/Fe	0.25	0.07	0.16	36	0.01	0.26
Si/Al	3.46	1.91	2.52	36	3.54	3.37
(μg/g)						
Sc	23	13	18	34	25	–
V	581	147	339	34	118	186
Cr	62	21	34	34	107	16
Co	116	60	90	34	8	84
Ni	404	43	108	34	36	281
Cu	62	10	39	34	26	37
Zn	111	32	62	34	59	–
As	419	23	159	34	11	687
Br	17	3	10	34	29	–
Rb	27	11	17	34	76	–
Sr	601	137	282	34	357	–
Zr	80	38	63	34	154	42
Nb	7	3	5	34	12	–
Mo	69	27	47	34	2	18
I	50	4	22	34	<d/l (4)	–
Ba	694	127	352	34	492	–
Pb	121	6	18	34	14	16
Bi	1	<d/l (1)	<d/l	34	2	–
Au	47	<d/l (0.01)	<d/l	10	–	–
Li	41	7	17	10	–	–
B	330	167	278	10	–	–
Th	7	2	4	34	9	–
U	9	1	4	34	3	–
La	16.60	8.20	12.23	24	39.9	6.2
Ce	30.50	16.40	22.98	24	66.2	12
Pr	3.30	1.80	2.53	24	11.3	2.5
Nd	11.70	6.70	9.09	24	30.7	8.2
Sm	2.60	1.40	1.99	24	6.26	2.5
Eu	0.65	0.30	0.47	24	1.34	–
Gd	2.50	1.30	1.88	24	5	–
Tb	0.50	0.21	0.34	24	0.55	–
Dy	3.30	1.50	2.26	24	4.2	0.5
Ho	0.86	0.34	0.56	24	0.79	–
Er	2.60	1.20	1.75	24	2.33	0.7
Tm	0.51	0.21	0.34	24	<dl (0.3)	–
Yb	3.30	1.50	2.34	24	2.3	0.6
Lu	0.69	0.27	0.45	24	<dl (0.3)	–

–: Without data. <d/l: less than detection limit.

are enriched in Mo, S and Pb, elements also contained in the framboidal and euhedral pyrites in the studied nodules. Mn oxides display major concentrations of Mn and high contents of Fe, Mg, Na, Ca and Ti. Al and Si are also abundant in the areas rich in Mn oxides (mottled to dendritic structure), probably related to the fine mixture between Mn oxides and clay minerals in these areas.

Detrital layers which contain a large proportion of terrigenous and biogenic material have high concentrations of terrigenous (Si, Al, Ti, K, Cr, Zr and Y) and biogenic (Ca and Mg) elements. Probably Zr is the best indicator of terrigenous contribution, which rises simultaneously with an increased content in detrital minerals in the nodules or in their layers.

4.5. Stable isotopic analyses

In general, the nuclei of the nodules show low depleted $\delta^{13}C$ values, ranging from −5.9 to −10‰ and the $\delta^{18}O_{PDB}$ varies from −2.8 to +3.8‰. The lowest values of $\delta^{13}C$ (as low as −10.03‰) correspond to calcite and dolomite (mean of $\delta^{13}C = -7.5$‰). This variability is also observed in their $\delta^{18}O$ values, the lowest corresponding to calcite (from −2.8 to 1.7‰) and the highest to dolomite (from 1.1 to 2‰). Siderite and rhodochrosite, the most abundant carbonates, show the highest values for carbon and oxygen isotopes. The values of $\delta^{13}C$ in siderite range from −5.9 to −7.1‰. Rhodochrosite presents values from −6.9 to −8.3‰. $\delta^{18}O$ values are from 2.8 to 3.3‰ in siderite and from 2.8 to 3.8‰ in rhodochrosite. There are no significant differences between the carbon and oxygen isotopic composition of siderites, rhodochrosites, dolomites and calcites from the different nuclei.

Framboidal pyrite aggregates show moderate to highly negative $\delta^{34}S_{CDT}$ isotopic values ranging between +13 and −41‰.

4.6. Organic carbon and biomarkers

The mean value for TOC analyzed in 14 bulk samples is 1.12% with contents ranging between 0.33 and 3.85%. The presence of biomarkers has been detected based on semi-quantitative analyses over powdered samples of the oxide layers from 10 nodules and nuclei from two nodules. Both, the nuclei and oxide layers present presence of the same biomarkers. Gas chromatograms (fragmentation ion $m/z = 57$) of the total hydrocarbon fraction show a similar pattern in all the studied samples, comprising a modal *n*-alkane distribution with a first concentration maximum at n–C_{18} and an important presence at n–C_{16} and n–C_{20}. Pristane and phytane and/or crocetane (2, 6, 11 and 15-tetrametilhexadecane) are present in all the samples analyzed. The chromatograms show a convex morphology known as unresolved complex mixture (UCM), characteristic of samples which have undergone an intense degree of marine microbial degradation. The lack of *n*-alkanes with large chains ($>n$–C_{25}) suggest absence or low input of terrestrial organic matter, or their intense degradation by bacterial activity. Moreover, the carbon preference index (CPI) ranges from 0.66 to 1.15, which is also characteristic of mature samples. In addition, phenanthrene was detected in all the nodules analyzed (fragmentation ion $m/z = 178$). This substance is not biological in origin and only occurs in petroleum and coals with a high degree of maturity. Fatty acids were detected in all the nodule samples composed of saturated acids (C_{14}–C_{18}) which indicates a bacterial origin. Organic sulphur was detected in the nucleus of one of the two nodules analyzed, indicating sulphate-reducing bacterial activity. The lipid Esqualene

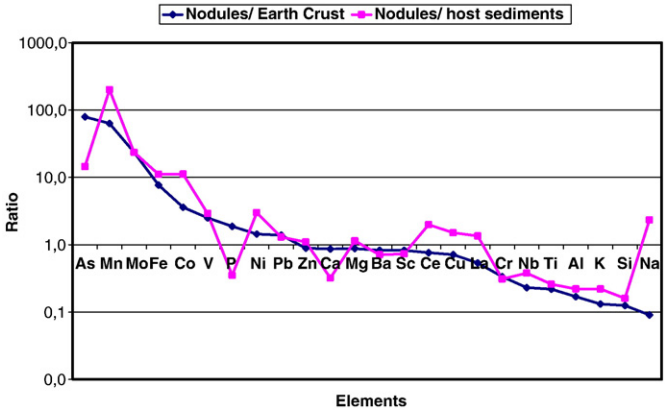

Fig. 8. Selected elements in Fe–Mn nodules from the Gulf of Cadiz compared to the mean contents of the Earth's Crust (Evans, 1980) and the mud-breccia host sediments. Elements above ratio line equal to 1 are enriched in the nodules.

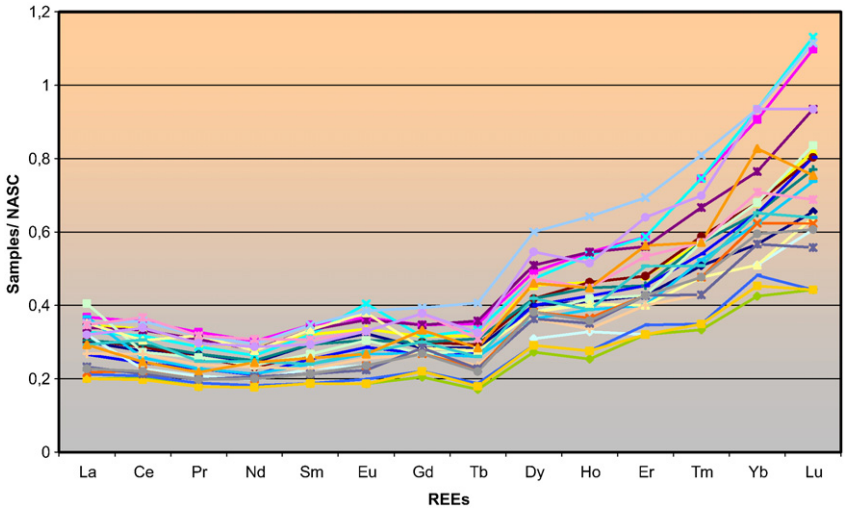

Fig. 9. Shale-normalized REE patterns of Fe–Mn nodules from the Gulf of Cadiz. All the samples display zero to slightly negative Ce anomaly, positive Eu anomaly and significant LREE/HREE fractionation. Shale values from Piper (1974).

is present in the nuclei and oxide layers as well as in archaea. Hop-17 (21)-ene hopane was not found in the oxide layers or nuclei of the nodules.

5. Discussion

The field sites, internal features, mineralogical and geochemical data from this study allow us to propose a comparison with other deep-seabed polymetallic nodules and shallow-water and continental margin nodules from other ocean basins and tectonic settings around the world. Moreover, based on these data we can discuss the genetic model of nodule growth in the oceanographic and geotectonic contexts of the Gulf of Cadiz.

5.1. Comparison with polymetallic deep-sea nodules, and shallow water and continental margin nodules

Polymetallic nodules are spreading in a wide variety of oceanographic and geotectonic contexts (e.g., Cronan, 1977; Hein et al., 1997; Jauhari and Pattan, 2000; Von Stackelberg, 2000; Baturin et al., 2002; Dekov and Savelli, 2004); nevertheless, marine ferromanganese oxide nodules around hydrocarbon seepage have not yet been reported. Therefore, the main distinctive characteristic of the studied nodules relative to other reported Fe–Mn nodule fields is their association with hydrocarbon-derived deposits and structures as carbonate chimneys and crusts, and carbonate-mud mounds in the GDR area. Moreover, the ferromanganese nodule fields are located in an area strongly influenced by the MOW action (physical–chemical conditions) and therefore the nodules can show these conditions as discussed below. The nodular physical properties such as maximum diameter, density, weight, and porosity are similar to those nodules reported from the Pacific and East Indian Ocean basins (e.g., Raab and Meylan, 1977; Von Stackelberg, 1997; Palma and Pessanha, 2000) and from shallow-waters and continental margins in the Baltic Sea, the Gulf of Finland, northern Russian seas and the Black Sea (e.g., Calvert and Price, 1977; Hlawatsch et al., 2002). Tabular to irregular morphologies are predominant in the studied nodules as in other shallow-water nodules such as those reported from the Kara and Baltic seas (Bogdanov et al., 1995; Glasby et al., 1997). Otherwise, cylindrical nodules are similar to the tubular concretions formed around burrows reported in the Black Sea (Baturin et al., 2002). The supply of different types of nucleus (soft sediment and hard clasts) may be related to the mud-breccia flows. Stuff clasts and mud from the mud-breccia flows could act as nucleation sites for the nodules in the areas dominated by extrusions from the mounds. The nodule shape could be related with the shape of the core. Tabular nodules generally have a tabular nucleus such as cylindrical nodules that grow around burrow tubes from seafloor sediment horizons.

As in other oceanic and continental margin nodules, the studied samples show a layered internal structure that at a macrotextural level is similar, but their microtextural features are distinctive from our nodules. Most of the oceanic and continental margin nodules show a colloform structure within the different typologies of macrotextures (massive, laminated, mottled, and columnar); hence their ferromanganese oxides are cryptocrystalline to amorphous (e.g., Von Stackelberg, 1997; Baturin et al., 2002). The studied nodules in the Gulf of Cadiz are characterized by displaying a micritic mosaic of rhombs of ferromanganese oxides at the microtextural level. These rhomboidal textures, included in a micro-crystalline matrix, are identical in the oxide layers and in the nucleus of the nodules, composed by siderite–rhodochrosite. We can use this petrographical feature to infer an initial common nature for both oxide layers and carbonate nuclei. Therefore the oxide layers can represent a postdepositional oxidation process that transforms siderite–rhodochrosite nodules into Fe–Mn oxide nodules. Carbonate cores correspond to the remains of the alteration process that modifies the carbonate nodule in an oxide nodule from the edges to the center. Moreover, the hydrocarbons present in the oxide layers and nuclei have the same nature.

The studied nodules are characterized by Fe oxyhydroxides (goethite type) predominating over Mn oxides unlike those in the deep-sea nodules where Mn oxides are dominant (e.g., Hein et al., 1997; Baturin et al., 2002). The silicates (clay minerals) present in the nodules are distinctive from the mud-breccia sediments with different sources than those of the hemipelagic samples (Martín-Puertas et al., 2007). The abundance of clay minerals (especially smectite) and their variety are therefore characteristic of the nodules from the Gulf of Cadiz in respect to other ferromanganese nodules, and directly related to the fluid venting processes. Carbonate minerals forming part of the oxide layers and nuclei are characteristic of the studied nodules unlike the majority of the ferromanganese nodules grown below the Carbonate Compensation Deep (CCD), in abyssal plains, where the carbonate mineral phases and nuclei are infrequent.

In comparison with the geochemical average values reported from deep-sea nodules (Baturin, 1988), the studied nodules have high Fe/Mn ratios >1, low trace metals and are enriched in Ca, Mg, Fe, C_{org} and As, although they are quite similar to those reported from the Black Sea (Baturin et al., 2002). Numerous authors have classified the oceanic nodules using the ternary diagram Mn–Fe— $(Cu + Ni + Co) \times 10$. According to this classification, nodules can be diagenetic with relations

Table 3
Pearson correlation matrix for major, minor and trace elements contained in the nodules from the Gulf of Cadiz.

	Al	Si	P	K	Na	Ca	Mg	Ti	Fe	Mn	Co	Ni	Cu	As	Mo	V	Zn	Pb	Sr	Ba	B	Li
Al	1.00	0.86**	−0.44**	0.88**	0.28	−0.45**	−0.41*	0.93**	−0.23	0.22	−0.49**	−0.15	0.14	−0.51**	−0.03	−0.31	−0.15	0.12	−0.26	−0.04	0.29	0.81**
Si	0.86**	1.00	−0.48**	0.86**	0.23	−0.45**	−0.42*	0.94**	−0.30	0.23	−0.35*	0.14	−0.01	−0.44**	−0.17	−0.31	−0.05	0.34	−0.25	−0.05	0.04	0.69*
P	−0.44**	−0.48**	1.00	−0.44**	−0.56**	0.51**	0.38*	−0.43**	0.37*	−0.68**	0.73**	0.11	0.14	0.93**	0.03	0.75**	0.63**	−0.16	0.07	−0.23	0.46	−0.64*
K	0.88**	0.86**	−0.44**	1.00	0.27	−0.49**	−0.28	0.89**	−0.22	0.22	−0.45**	−0.11	0.15	−0.44**	−0.07	−0.20	−0.12	0.15	−0.33	−0.03	0.30	0.80**
Na	0.28	0.23	−0.56**	0.27	1.00	−0.43**	−0.56**	0.18	−0.01	0.33*	−0.31	−0.28	0.36*	−0.41*	0.06	−0.46**	−0.56**	−0.28	−0.07	−0.03	−0.38	0.69*
Ca	−0.45**	−0.45**	0.51**	−0.49**	−0.43**	1.00	0.53**	−0.41*	−0.31	−0.36*	0.61**	0.52**	−0.36*	0.41*	0.05	0.30**	0.37*	−0.07	0.30	−0.08	0.26	−0.72*
Mg	−0.41*	−0.42*	0.38*	−0.28	−0.56**	0.53**	1.00	−0.36*	−0.36*	−0.15	0.16	0.17	−0.18	0.33	−0.18	0.46**	0.34*	0.10	−0.12	−0.06	−0.19	−0.32
Ti	0.93**	0.94**	−0.43**	0.89**	0.18	−0.408*	−0.36*	1.00	−0.27	0.20	−0.38*	0.03	0.01	−0.44**	−0.08	−0.22	−0.02	0.32	−0.25	−0.04	0.33	0.71*
Fe	−0.23	−0.30	0.37*	−0.22	−0.01	−0.31	−0.36*	−0.27	1.00	−0.57**	0.29	−0.39*	0.41*	0.29	0.08	0.09	0.09	−0.24	−0.17	−0.28	0.66*	−0.11
Mn	0.22	0.23	−0.68**	0.22	0.33*	−0.36**	−0.15	0.20	−0.57**	1.00	−0.73**	−0.13	−0.19	−0.53**	0.24	−0.27	−0.51**	0.18	0.39*	0.70**	−0.63	0.39
Co	−0.49**	−0.35*	0.73**	−0.45**	−0.31	0.61**	0.16	−0.38*	0.29	−0.73**	1.00	0.51**	0.00	0.74**	0.03	0.47**	0.60**	0.05	−0.06	−0.31	0.46	−0.71*
Ni	−0.15	0.14	0.11	−0.11	−0.28	0.52**	0.17	0.03	−0.39*	−0.13	0.51**	1.00	−0.42*	0.17	0.05	0.13	0.45**	0.41*	0.01	−0.05	−0.16	−0.57
Cu	0.14	−0.01	0.14	0.15	0.36*	−0.36*	−0.18	0.01	0.41*	−0.19	0.00	−0.42*	1.00	0.15	−0.02	0.13	0.06	−0.41*	−0.25	−0.17	−0.33	0.31
As	−0.51**	−0.44**	0.93**	−0.44**	−0.41*	0.41*	0.33	−0.44**	0.29	−0.53**	0.74**	0.17	0.15	1.00	0.09	0.82**	0.65**	−0.10	0.17	−0.11	0.28	−0.57
Mo	−0.03	−0.17	0.03	−0.07	0.06**	0.05	−0.18*	−0.22	0.08	0.24	0.03	0.05	−0.02	0.09	1.00	0.26	0.10	0.11	0.43*	0.50**	0.42	0.10
V	−0.31	−0.31	0.75**	−0.20	0.46**	0.30	0.46**	−0.22	0.09	−0.27	0.47**	0.13	0.13	0.82**	0.26	1.00	0.68**	0.15	0.19	0.08	0.35	−0.45
Zn	−0.15	−0.05	0.63**	−0.12	−0.56**	0.37*	0.34*	−0.02	0.09	−0.51**	0.60**	0.45**	0.06	0.65**	0.10	0.68**	1.00	0.17	−0.12	−0.23	0.29	−0.62
Pb	0.12	0.34	−0.16	0.15	−0.28	−0.07	0.10	0.32	−0.24	0.18	−0.06	0.41*	−0.41*	−0.10	0.11	0.15	0.17	1.00	−0.08	0.02	−0.02	−0.20
Sr	−0.26	−0.25	0.07	−0.33	−0.07	0.30	−0.12	−0.25	−0.17	0.39*	0.05	0.01	−0.25	0.17	0.43*	0.19	−0.12	−0.08	1.00**	0.76**	0.13	−0.30
Ba	−0.04	−0.05	−0.23	−0.03	−0.03	−0.08	−0.06	−0.04	−0.28	0.70**	−0.31	−0.05	−0.17	−0.11	0.50**	0.08	−0.23	0.02	0.76**	1.00	−0.13	−0.06
B	0.29	0.04	0.46*	0.30	−0.38	0.26	−0.19	0.33*	0.66*	−0.63	0.46	−0.16	−0.33	0.28	0.42	0.35	0.29	−0.02	0.13	−0.13	1.00	0.13
Li	0.81**	0.69**	−0.64*	0.78**	0.69*	−0.72*	−0.32	0.71*	−0.11	0.39	−0.71*	−0.57	0.31	−0.57	0.10	−0.45	−0.62	−0.20	−0.30	-0.06	0.13	1.00

** The correlation is significant at the 0.01 level.
* The correlation is significant at the 0.05 level.

Mn/Fe > 2.5 rich in Cu and Ni and poor in Co; hydrogenetic in which Mn/Fe ≅ 1 and there are relatively high concentrations of Cu + Ni + Co in respect to the other genetic types; and hydrothermal where Mn/Fe is either very high or very low and the nodules normally have low Cu + Ni + Co (Bonatti et al., 1972; Lyle, 1981; Dymond et al., 1984; Fitzgerald and Gillis, 2006). The nodules studied in this work present Mn/Fe < 0.25 and low contents of Co, Ni, Cu and REEs in all samples. In the same way, there are abundant references about nodules from shallow waters and continental margins where Fe, Mn and trace metal contents are rather similar to the nodules from the Gulf of Cadiz (Calvert and Price, 1977; Boström et al., 1982; Ingri, 1985; Glasby et al., 1997; Baturin et al., 2002). All of them display very low Mn/Fe ratios as a result of their growth by combined diagenetic–hydrogenous processes. In addition, the contents in some elements in the nodules from the Gulf of Cadiz (V, As, Ca, Mg, Ni, Co and Mo) are more similar to those obtained in the shallow-water nodules from the Baltic or Black seas (e.g., Volkov, 1979) than to those in deep-sea nodules. In this sense, the average growth rate of the studied nodules must be very fast, as occurs in the Baltic Sea nodules with average rates of 20,000 mm Myr^{-1} (Zhamoida et al., 1996; Hlawatsch et al., 2002). These growth rates are several orders of magnitude higher than those frequently found in hydrogenous deep-sea nodules and crusts (av. 1–6 mm Myr^{-1}) (Hein, 2001). Therefore, fast growth rates emphasize the importance of sediment diagenetic processes (Reyss et al., 1982). Furthermore, this relatively rapid accretion is probably one of the main causes of the overall low contents of transition metals in these continental margin nodules. The positive correlation coefficient between Mn and Na, Ca, Mg, Ba and Sr in bulk sample and/or individual layers may be attributed to the stabilization of the birnessite–jianshuite structures by monovalent and divalent cations as numerous researchers describe in other works (Burns and Burns, 1977; Bischoff et al., 1981). As in other oceanic manganese deposits (e.g., Burns and Burns, 1979), the mineralogy of Fe–Mn oxides in the studied nodules has been considered to be the main seat of heavy metals.

The organic carbon contained in the studied samples (av. 1.12%) is substantially higher than in deep-sea polymetallic nodules (av. 0.1%; Baturin, 1986), but quite similar to ferromanganese concretions from the Black Sea (av. 0.7%; Baturin et al., 2002). Furthermore, the oxide layers of the studied nodules contain mature hydrocarbons derived from bacterial activity, with the presence of aromatic hydrocarbons as phenanthrene, characteristic of mature petroleum.

SEM observations in carbonate minerals (siderite–rhodochrosite) from the nuclei of Fe–Mn nodules, with well developed idiomorphic to sub-idiomorphic rhombohedra crystals, and $\delta^{13}C$ low values (as low as −10‰ PDB), can be interpreted as evidence of the important involvement of microbial activity in the formation of these authigenic carbonates within the sediment column at the place where the nodules are growing. The carbon isotopic composition of these carbonates can be related to the mixing of different carbon sources: carbon derived from methanogenesis, methane oxidation, fermentation of organic matter, dissolved carbonate tests and sea water.

5.2. Origin of the nodules: influence of the oceanographic and geotectonic framework

The Gulf of Cadiz is located in the present compressive boundary of the Eurasian and African plates (Dewey et al., 1989), displaying a strong deformation in relation to the prevailing tectonic activity, diapirism, structures of fluid seep, and slidings (Medialdea et al., 2004). Nodule fields appear in an area where the geological, oceanographic and biological processes have an important interrelation. This area is affected by different structures and deposits related to fluid venting such as the GDR and their hydrocarbon-derived carbonated deposits (chimneys and crusts). Mn nodule fields extend across large surfaces, probably related with areas of discharge of fluids from fault systems in the flanks and the base of extrusive edifices from the GDR. Topographic highs as GDR may act as sites for crustal discharge of fluids and the consequent

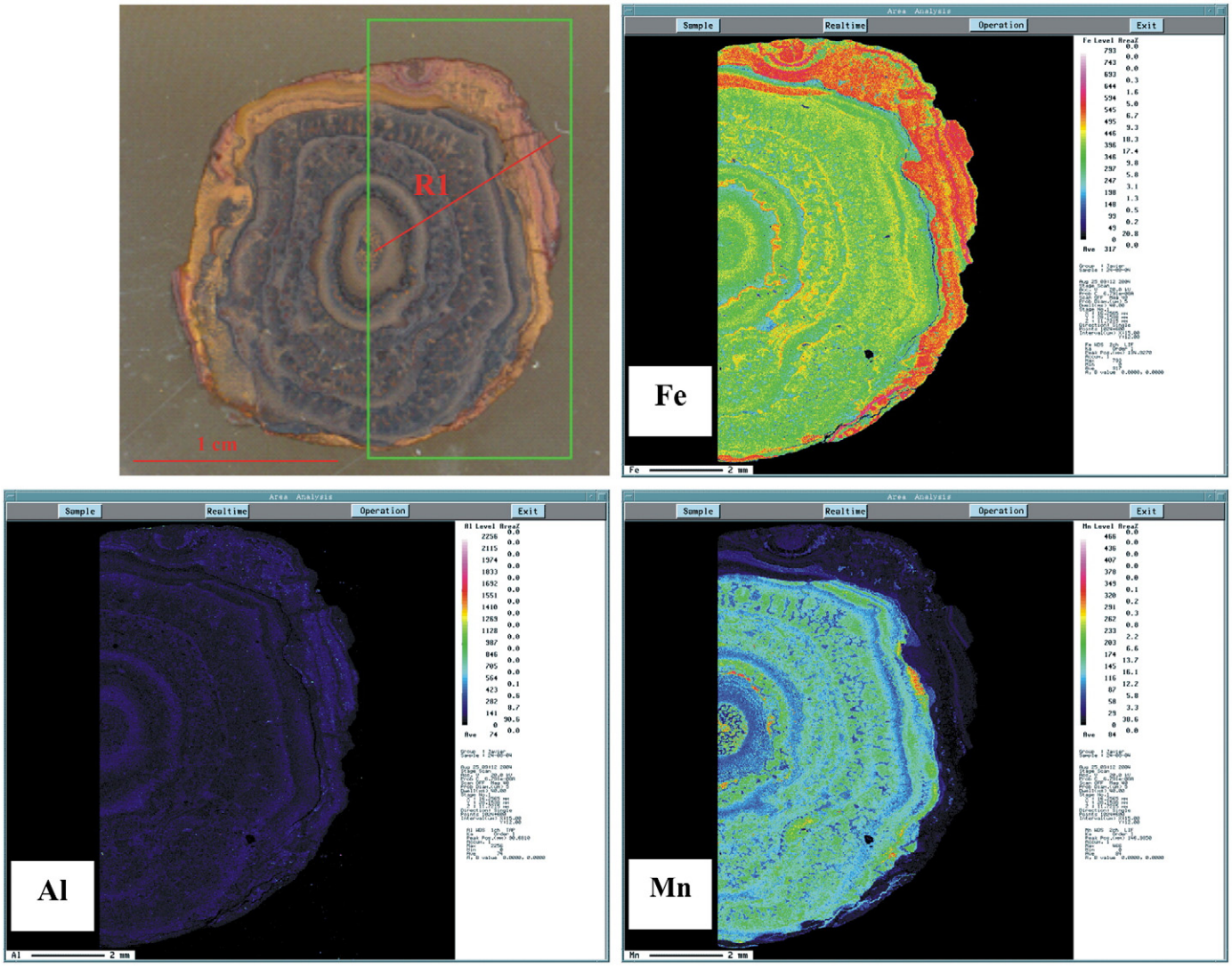

Fig. 10. Fe, Mn and Al EPMA mapping distribution in the nodule ANAS01/D19-01. Cool colors indicate low contents, warm colors indicate high contents of these elements. We can observe the concentric growth pattern of layers and the special enrichment in Fe in the external part of the nodule, affected by alteration front discontinuity (orange layers).

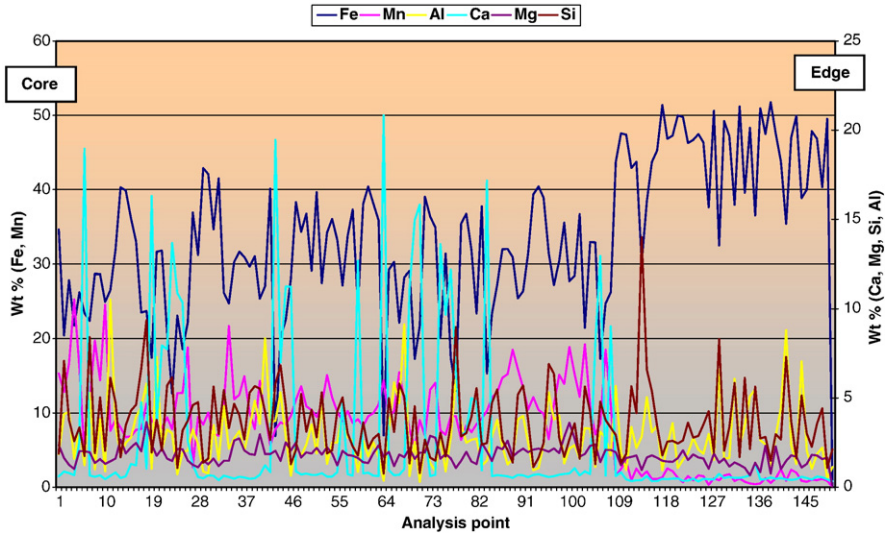

Fig. 11. EPMA distribution for Fe, Mn, Ca, Si, Al and Mg across the R1 profile (Fig. 10) every 50 μm from the core to the external edge in a sub-spherical nodule. Fe, Mn and Ca may show a certain cyclicity in their patterns. It can be related to the MOW and NADW water masses interaction.

accumulation of mineral deposits and development of vent-associated faunal communities. Numerous authors have reported these phenomena in other oceanic areas around the world (e.g., Alt, 1988; Mottl et al., 1998). Mud volcanoes and diapiric ridges present large heat flow and geochemical anomalies with respect to the surrounding area and related with faulting structures (Gardner, 2001). These structures facilitate fluid flow between deep crustal materials and the ocean, with mud volcanoes and diapiric ridges being the expression of crustal fluid discharge, and probably recharge sites for seawater. Fluid venting across these fault systems could facilitate the mature hydrocarbon migration from deep-seated reservoirs to the seafloor. These mature hydrocarbons located within the nodules have also been found within the methane-derived carbonate chimneys and crusts from the area (González et al., in prep.); therefore, they are impregnating all the superficial sediments in the seep-areas. In addition, mature hydrocarbon gases ($Ro < 1.2\%$) derived from kerogen type II and a mixture of kerogens of types II and III have been reported from sediments in the Moroccan mud volcano province of the Gulf of Cadiz (Stadnitskaia et al. 2006). The presence of phenanthrene and mature hydrocarbons in the studied samples suggests that thermogenic hydrocarbons have migrated to the area, and therefore may be contributing to the generation of carbonates. The fractionation of carbon might be conditioned by the oxidation of these hydrocarbons in their reservoirs and by the migration process across fractures from deep seated sources or reservoirs to the seafloor. In this framework of oxidizing seawaters, carbonate formation induced by anaerobic oxidation of methane (AOM) is confined to anoxic sediment layers that are later exposed by erosional processes (e.g., Jørgensen, 1989; Stakes et al., 1999; Peckmann et al., 2001). Therefore, the current position of the dolomite to ankerite chimneys and crusts, lying on the seafloor, seems to point to their exhumation by bottom current activity of the MOW. In this sense, nodules and carbonate chimneys and crusts represent cementations over mudstone to sandstone sediments (essentially mud-breccia) derived from the extrusive episodes in the mud mounds and volcanoes. These cementations occur beneath the sediment–water interface, sometimes mediated by microorganisms. Microbiological synthesis of oxides, carbonates and sulphides in nodules and sediments has been reported by numerous authors (e.g., Hein and Koski, 1987; Nealson and Myers, 1992; Kohn et al., 1998; Stein et al., 2001). Microorganisms such as archaeas, sulphate-reducing bacteria and sulphide-oxidizing bacteria have been found in sediments and carbonates from mud volcanoes and mud-carbonate ridges in the Gulf of Cadiz (e.g., Niemann et al., 2006). These organisms use the hydrocarbon-enriched fluids from seeps in their vital activity, giving rise directly or indirectly to the following minerals: carbonates and sulphides in anoxic environments (by archaeas and SRB respectively) and oxides in oxidizing environments (by sulphide-oxidizing bacteria). Pyrites from the nodules exhibit textural (clots and framboids), geochemical (abundance of organic sulphur and C_{org}) and isotopic ($\delta^{34}S_{CDT}$ between $+13$ and $-41‰$) values, typical characteristics of microbial-mediated pyrite, formed by anoxic oxidation of methane through a syntrophic interaction between methanotropic archaea and sulphate-reducing bacteria (SRB) (Hinrichs and Boetius, 2002). The idiomorphic crystals of Fe–Mn carbonates from the nodular nuclei indicate recrystallization processes that occurred after the mud extrusion within the mud flows, reducing sediment. These carbonate crystals present a void in their central position that probably corresponds to the archaea cell cast, also observed in hydrocarbon-derived carbonate chimneys from the area. Therefore, filamentous and bulbous textures observed in Fe–Mn oxides in the nodules could have been generated by sulphide-oxidizing bacteria within the upper oxidizing sediment. Moreover, the existence of low molecular saturated fatty acids (C_{14}–C_{18}), whose content usually sharply decreases during burial, indicates recent bacterial participation in the organic matter formation, probably linked with bacterial mineralization processes. Fatty acids present as bacterial markers in Fe–Mn nodules from the Pacific and Indian oceans are related to the genetic types and element distribution in those deposits (Aleksandrova and Poluyaktov, 1996).

The GDR area is affected by strong erosive processes linked to the MOW action. In this context there are various features in the studied samples that probably are related to the MOW influence. The presence of previous detrital layers and burrows enclosed within the nodules from the Gulf of Cadiz may indicate that they could have been formed beneath the sediment–water interface and later exposed by erosion as occurs with carbonate chimneys and crusts. In this area the MOW undercurrent is characterized by current velocities of 20–30 cm/s (Hernández-Molina et al., 2006). Variations in the metal content in respect to nodule sizes have been observed by numerous authors in different oceanic areas (Von Stackelberg, 2000; Jauhari and Pattan, 2000). They seem to be related to the intervention of various processes of nodular accretion (diagenetic, hydrothermal and hydrogenetic). In the nodules studied, we cannot observe any apparent correlation between metal contents and nodules sizes. Therefore we can understand that the diagenetic process for the nodular accretion is dominant in the area studied, the other growth models being less important. According to Von Stackelberg (2000), the dendritic and dense laminated textures observed in our samples are characteristic of diagenetic growth within the sediment. The strong Fe-enrichment observed in the studied nodules versus deep-sea concretions may be explained as a consequence of pyrites and Fe-rich carbonates from sediment being the primary source of Fe. Furthermore, MOW could have been rich in Fe and Mg, especially in the glacial periods, where the lower sea level permitted sufficient input of fluvial waters carried with elevated Fe concentrations (Hamoumi and Chafik, 2006; Kozlova et al., 2007) and probably the MOW's action over the oxidizing superficial sediment covered the clastic grains with Fe covers. These covers could be another Fe source for the generation of Fe-carbonates. Fe-enrichments of the MOW in the glacial periods could be the reason for the external Fe-enrichments in the studied nodules. On the other hand, the nodules studied are depleted in Mn in the outer layers affected by the alteration front, probably formed after the exhumation. This fact is explained by the high geochemical mobility of Mn as a response to changes in the environment conditions. Thus, the chemistry of the MOW in the area, which is characterized by low values of dissolved oxygen in the water (160–170 μmol/kg) (Cabeçadas et al., 2002) could have contributed, together with the intense undercurrent, to the depletion of Mn from the outer layers in the exhumed nodules. In contrast, these outer layers are Fe-rich, indicating a recent period of stagnation in the nodule growth. This is coherent with an intense erosive action of the lower core of the MOW in the glacial stages, the most active core in these periods, permitting Fe–Mn nodules to appear uncovered by sediments. The high porosity observed in these outer layers reflects a dissolution process also related to changes in the geochemistry of the environment. In nodules from the Central Indian Ocean Basin, Jauhari and Pattan (2000) found Fe and Co concentrated close to the nucleus (hydrogenetic in origin), and Mn more concentrated in the exterior layers (early diagenetic). In the nodules studied here we can observe Mn more concentrated in the exterior layers in some samples without the development of alteration front. It could be related to diagenetic post-depositional processes (growing of dendritic structures across fractures) and recent exhumation. Zero to negative Ce anomaly in the studied nodules suggests that they were formed at a lower redox level in the vicinity of the redox boundary, and in agreement with a diagenetic growth and later exhumation process. Positive Eu anomalies could be related to mineral precipitation from fluids with a hydrothermal component in a reduced environment. The presence of detrital Na-feldspar or aeolian Saharan dust contained within the nodules could also be related to the Eu anomaly.

As reported from other shallow-water concretions (e.g., Loch Fyne, Scotland; British Columbia; Baltic Sea), the nodules recovered from the Gulf of Cadiz are found lying over brown oxidized sediments, whereas their subsurface sediments, ranging from a few millimeters to a few centimeters in depth, consist of olive-grey reduced muds containing H_2S and sulphides (Somoza et al., 2003). Textural equilibrium observed between rhombohedra oxide crystals and pyrite framboids (partial or

totally pseudomorphised by goethite) points out that both crystalline structures, rhomboidal and framboidal were formed at the same time and therefore, both are syn-genetic. However, redox conditions necessary for pyrite and oxide formation are radically different. Presently, in this area, carbonates and pyrites grow jointly at a depth of 20–200 cm below the sea floor within the sulphate–methane transition zone (SMT) under anaerobic conditions as a consequence of the microbial-mediated methane oxidation and sulphate reduction (Niemann et al., 2006). Our observations suggest that crystals of goethite–Mn oxides are derived from carbonates (siderite to rhodochrosite) in origin, where the contribution of different carbon sources such as hydrocarbon and bacterial oxidation of organic matter must be important. In this way, the rhombic oxide crystals represent pseudomorphs of carbonate micritic crystals originated by diagenetic transformations from Fe–Mn carbonates to Fe–Mn oxides under oxidizing conditions. Similar textures and primary associations of pyrite-carbonates have been observed in mud-breccia, high-sulphide sediments ejected by fluid venting (Martín-Puertas et al., 2006); and in hydrocarbon-derived carbonate chimneys from the Gulf of Cadiz (e.g., Díaz-del-Río et al., 2003; González et al., 2006b). In addition, goethite replacements of carbonates have been observed in burial corals from mud diapiric ridges in the Gulf of Cadiz (Kozlova et al., 2007). Carbon dioxide produced by the transformation of carbonates to oxides could have generated fluidification discontinuities observed in the oxide layers. As a result of the strong erosive action of the sea-bottom undercurrents, Fe-sulphides formed within a highly reduced zone only a few centimeters below sediments may be in contact with suboxic to oxic interstitial water from oxidizing oceanic-bottom waters. The exhumation process leads to oxidation of Fe^{2+} to Fe^{3+} and of Mn^{2+} to Mn^{3+} and Mn^{4+}, thus forming the Fe–Mn oxyhydroxides. Therefore, different factors could control the nodule growth, such as supply of metals from pore sediments, intensity of diagenetic processes, Eh potential, microbiological activity and erosive action of bottom currents.

The presence of a second generation of sulphides and kutnahorite precipitates that are filling pores and cracks of nodules implies the existence of reduced micro-niches in an oxic environment. Reduced micro-niches with sulphide precipitates have been observed in Fe–Mn nodules in other areas (e.g., Baturin, 1986).

Mn-rich and Mn–Fe mixed layers may represent active growth beneath the sediment–water interface in the vicinity of the redox boundary, Mn and Fe being directly supplied from sediment pore waters. Fe-rich layers are related to periods of exposition to the bottom waters with very low growth rates, Fe-oxides precipitated from the seawater and Mn removed from the external part of the nodules.

6. Summary and conclusions

In this paper we report detailed textural, mineralogical and geochemical characteristics of Fe–Mn nodules discovered and sampled in the continental margin of the Gulf of Cadiz. The area is characterized by an abundance of fluid venting related structures (mud volcanoes, diapirs, pockmarks and carbonate chimneys) and the strong influence of the Mediterranean Outflow Water undercurrent in the modeling and configuration of the continental margin. The nodule fields extend along the mid-continental slope at an average depth of 900 m at the base and flanks of a sequence of carbonate-mud mounds named the Guadalquivir Diapiric Ridge that acts as a barrier for the Mediterranean outflow bottom current (Díaz-del-Río et al., 2003). Nodules were found together with large amounts of hydrocarbon-derived chimneys and crusts and mud-breccia deposits related to fluid venting of deep-seated hydrocarbons on the sea floor through faults and sediment pores in this area (e.g., Somoza et al., 2002; León et al., 2007).

The nodules, fundamentally tabular–irregular in morphology, grow concentrically around a nucleus of Miocene blue marls and sediments ejected by fluid venting from the underlying units of the so-called "Olistostrome Mass" (Maldonado et al., 1999). Internally, nodules consist of layers, clearly concentric in small nodules, but forming complex morphologies in large and composite nodules where it is possible to distinguish growing, fracture, burrowing and alteration discontinuities. The textures developed by the layers are massive, laminated, detritic and mottled to dendritic. The nuclei are composed of a micritic mosaic of siderite–rhodochrosite rhombic crystals with minor quantities of silicates and other carbonates. The layers show the same microtextural rhombic features but are formed by Fe–Mn oxyhydroxides. These oxides display crystals of a relatively big size regarding cryptocrystalline Fe–Mn oxides from other shallow or deep ocean nodules. Quartz and phyllosilicates (detrital) are commonly present, although in much smaller proportion, than the Fe–Mn oxyhydroxides. Nodules show a quite similar geochemistry with shallow-water nodules rather than deep-sea polymetallic nodules. They display a high mean abundance of Fe (38.6%), moderate Mn (6.0%), and low contents of trace metals and REEs.

For nodule genesis we propose both diagenetic and hydrogenous processes, beneath and on seabed sediment, as a consequence of alternating episodes of burial and exhumation, and due to the bottom current activity of the MOW. The presence of mature hydrocarbons such as phenanthrene within the nodules indicates that diagenetic processes are related to deep-seated hydrocarbon seeps, probably through microbial-mediated anaerobic oxidation of hydrocarbons. On the other hand, the variability in the hydrogenous nodule growth may be related to the interface between the oxygenated North Atlantic deep waters and the briny Mediterranean outflow waters. This action was more intensive in the glacial periods, when the lower core of the MOW was the most active and this increased the erosive undercurrent action in the area, giving rise to the exhumation of nodules and precipitation of Fe-oxides from seawater.

Future detailed geochemical, chronological and isotopic analyses from the core to the edges of Fe–Mn nodules may provide us information about the evolution of the MOW and its action in the area throughout the time of nodule generation.

Acknowledgements

This work has been funded thanks to a research fellowship of the Geological Survey of Spain within the framework of the European Science Foundation's EuroCORE–EuroMARGINS projects: "MOUNDFORCE" (O1-LEC-EMA06F, REN-2002-11668-E-MAR) and "MVSEIS" (O1-LEC-EMA24F, REN-2002-11669-E-MAR). The investigation is also supported by the Spanish Interministry Commission of Science and Technology (CICYT) project CONTOURIBER (CTM2008-06399-C04/MAR), and the Consolider-Ingenio 2010 Programme, under project CSD2006-0041, Topolberia. The authors wish to thank all the scientific and technical personnel who participated in the oceanographic cruises of the "TASYO" project, of the R/V "*Cornide de Saavedra*" and R/V "*Hespérides*", for the data acquisition and their expertise in collecting the samples. We would also like to thank the facilities for the use of their equipment, the personnel of the "Centro de Microscopía Electrónica y Citometría", "Universidad Complutense de Madrid" (UCM), "Centro de Astrobiología" (CSIC/INTA), "Laboratorio de Estratigrafía Biomolecular" (UPM), "Laboratorio de Isótopos Estables" (USAL), and the laboratories of the "Instituto Geológico y Minero de España" (IGME). Two anonymous reviews and Editors helped improve the clarity and focus of this contribution.

References

Abouchami, W., Galer, S.J.G., Koschinsky, A., 1999. Pb and Nd isotopes in NE Atlantic Fe–Mn crusts: proxies for trace metal paleosources and paleocean circulation. Geochimica et Cosmochimica Acta 63, 1489–1505.

Al-Aasm, I., Taylor, B.E., South, B., 1990. Stable isotope analysis of multiple carbonate samples using selective acid extraction. Chemical Geology. Isotope Geoscience Section 80, 119–125.

Alt, J.C., 1988. Hydrotermal oxide and nontronite deposits on seamount in the eastern Pacific. Marine Geology 81, 227–239.

Aleksandrova, O.A., Poluyaktov, V.F., 1996. Fatty acid composition of the iron–manganese nodules and surrounding sediments in the Pacific and Indian oceans. Oceanology 35 (5), 630–637.

Ambar, I., Howe, M.R., 1979a. Observations of the Mediterranean Outflow I. Mixing in the Mediterranean Outflow. Deep-Sea Research 26A, 535–554.

Ambar, I., Howe, M.R., 1979b. Observations of the Mediterranean Outflow II. The deep circulation in the vecinity of the Gulf of Cadiz. Deep-Sea Research 26A, 555–568.

Baraza, J., Ercilla, G., 1996. Gas-charged sediments and large pockmark like features on the Gulf of Cadiz slope (SW Spain). Marine and Petroleum Geology 13 (2), 253–261.

Baturin, G.N., 1986. Geochemistry of Oceanic Ferromanganese Nodules. Nauka, Moscow.

Baturin, G.N., 1988. The Geochemistry of Manganese and Manganese Nodules in the Ocean. D. Riedel Publ. Co. 342 pp.

Baturin, G.N., Gorshkov, A.I., Magazina, L.O., Bogdanova, O.Yu., 2002. Structure and composition of ferromanganese–phosphate nodules from the Black Sea. Lithology and Mineral Resources 37 (4), 374–385.

Bischcoff, J.C., Piper, D.Z., Leong, K., 1981. The aluminosilicate fraction of North Pacific manganese nodules. Geochimica et Cosmochimica Acta 45, 2047–2049.

Bogdanov, Yu.A., Gurvich, E.G., Bogdanova, O.Yu., Ivanov, G.V., Isaeva, A.B., Muravév, K.G., Gorshkov, A.I., Dubinina, G.I., 1995. Ferromanganese nodules of the Kara Sea. Oceanology 34 (5), 722–732.

Bonatti, E., Kraemer, T., Rydell, H., 1972. Classification and genesis of submarine iron–manganese deposits. In: Horn, D.R. (Ed.), Ferromanganese Deposits of the Ocean Floor. Arden House, New York, pp. 149–165.

Boström, K., Wiborg, L., Ingri, J., 1982. Geochemistry and origin of ferromanganese concretions in the Gulf of Bothnia. Marine Geology 50, 1–24.

Burns, R.G., Burns, V.M., 1979. Manganese oxides. In: Burns, R.G. (Ed.), Marine Minerals, Reviews in Mineralogy. Washington, D.C., Min. Soc. Am. vol. 6, pp. 1–46.

Burns, V.M., Burns, M.G., 1977. Mineralogy. Marine Manganese Deposits: In: Glasby, G.P. (Ed.), Elsevier Oceanography Series, 15. Amsterdan, pp. 185–248.

Cabeçadas, G., Brogueira, M.J., Gonçalves, C., 2002. The chemistry of Mediterranean outflow and its interactions with surrounding waters. Deep-Sea Research. Part 2. Topical Studies in Oceanography 49, 4263–4270.

Calvert, S.E., Price, N.B., 1977. Shallow water, continental margin and lacustrine nodules: distribution and geochemistry. Marine Manganese Deposits: In: Glasby, G.P. (Ed.), Elsevier Oceanography Series, Amsterdam, pp. 45–86.

Claude, C., Suhr, G., Hofmann, A.W., Koschinsky, A., 2005. U–Th chronology and paleoceanographic record in Fe–Mn crusts from the NE Atlantic over the last 700 ka. Geochimica et Cosmochimica Acta 69, 4845–4854.

Coleman, M.L., Moore, M.P., 1978. Direct reduction of sulfates to sulfur dioxide for isotopic analysis. Analytical Chemistry 50 (11), 1594–1595.

Cronan, D.S., 1977. Deep-sea nodules: distribution and geochemistry. Marine Manganese Deposits: In: Glasby, G.P. (Ed.), Elsevier Oceanography Series, Amsterdam, pp. 11–44.

Dekov, V.M., Savelli, C., 2004. Hydrothermal activity in the SE Tyrrhenian Sea: an overview of 30 years of research. Marine Geology 204, 161–185.

Dewey, J.F., Helman, M.L., Turco, E., Hutton, D.H.W., Knott, S.D., 1989. Kinematics of the Western Mediterranean: Alpine Tectonics: In: Coward, M. (Ed.), Special Publication Geological Society of London, London, vol. 45, pp. 265–283.

Díaz-del-Río, V., Somoza, L., Martinez-Frias, J., Hernandez-Molina, F.J., Lunar, R., Fernandez-Puga, M.C., Maestro, A., Terrinha, P., Llave, E., Garcia, A., Garcia, A.C., Vazquez, J.T., 2001. Carbonate chimneys in the Gulf of Cadiz: initial report of their petrography and geochemistry. Final Proc. Int. Conf. Geological Processes on Deep-Water European Margins, Moscow, Russia: UNESCO IOC Workshop Report, vol. 175, pp. 53–54.

Díaz-del-Río, V., Somoza, L., Matínez-Frías, J., Mata, M.P., Delgado, A., Hernández Molina, F.J., Lunar, R., Martín Rubí, J.A., Maestro, A., Fernádez Puga, M.C., León, R., Llave, E., Medialdea, T., Vazquez, J.T., 2003. Vast field of hydrocarbon-derived carbonate chimneys related to the accretionary wedge/olistostrome of the Gulf of Cadiz. Marine Geology 195, 177–200.

Dymond, J., Lyle, M., Finney, B., Piper, D.Z., Murphy, K., Conard, R., Pisias, N., 1984. Ferromanganese nodules from MANOP Sites H, S and R — control of mineralogical and chemical composition by multiple accretionary processes. Geochimica et Cosmochimica Acta 48, 931–950.

Eisenhauer, A., Gögen, K., Pernicka, E., Mangini, A., 1992. Climatic influences on the growth rates of Mn crusts during Late Quaternary. Earth Planetary Science Letters 109, 25–36.

Evans, A.M., 1980. An Introduction to Ore Geology. Blackwell Scientific Publication, Oxford. 356 pp.

Faugères, J.-C., Gonthier, E., Stow, D.A.V., 1984. Contourite drift molded by deep Mediterranean outflow. Geology 12, 296–300.

Fernández Puga, M.C. 2004. Diapirismo y estructuras de expulsión de gases hidrocarburos en el talud continental del Golfo de Cádiz. Tesis Doctoral. Universidad de Cadiz. 335 pp.

Fitzgerald, C.E., Gillis, K.M., 2006. Hydrothermal manganese oxide deposits from Baby Bare seamount in the Northeast Pacific Ocean. Marine Geology 225, 145–156.

Fomina, L.S., Volkov, I.I., 1969. Rare earths in iron–manganese concretions of the Black Sea. Doklady Akademii Nauk SSSR 185, 158–161.

Gardner, J.M., 2001. Mud volcanoes revealed and sampled on the Moroccan continental margin. Geophysical Research Letters 28 (2), 339–342.

Gardner, J.V., Kidd, R.B., 1987. Sedimentary processes on the Iberian continental margin viewed by long-range side-scan sonar and seismic data. Journal of Sedimentary Petrology 57 (3), 397–407.

Glasby, G.P., (Ed.) 1977. Marine Manganese Deposits. Elsevier Oceanography Series, 15. Amsterdan. 523 pp.

Glasby, G.P., Emelyanov, E.M., Zhamoida, V.A., Baturin, G.N., Leipe, T., Bahlo, R., Bonacker, P., 1997. Environments of formation of ferromanganese concretions in the Baltic Sea: a critical review. Manganese Mineralization: Geochemistry and Mineralogy of Terrestrial and Marine Deposits: In: Nicholson, K., Hein, J.R., Bühn, B., Dasgupta, S. (Eds.), Special Publication Geological Society of London, London, vol. 119, pp. 213–237.

González, F.J., Somoza, L., Lunar, R., Martínez-Frías, J., Martín Rubí, J.A., Díaz-del-Río, V., 2006a. Nódulos de Fe–Mn: El nuevo descubrimiento del Golfo de Cádiz. Boletín Geológico y Minero 117, 491–497.

González, F.J., Pinheiro, L.M., Magalhães, V.H., Ivanov, M., Somoza, L., Merinero, R., 2006b. Sulphate-reducing bacteria as a nucleation sites for pyrite in carbonate chimneys from the Vernadsky Ridge, Moroccan margin of the Gulf of Cadiz. Final Proc. Int. Conf. Geological Processes on Deep-Water European Margins, Moscow, Russia: UNESCO IOC Workshop Report, vol. 201, pp. 19–22.

González, F.J., Somoza, L., Lunar, R., Martínez-Frías, J., Martín Rubí, J.A., Torres, T., Ortiz, J.E., Díaz-del-Río, V., 2007. Fe–Mn nodules associated with hydrocarbon seeps: a new discovery in the Gulf of Cadiz. Episodes 30 (3), 187–196.

Hamoumi, N., Chafik, M., 2006. Tubotomaculum of NW Rift Belt: mode of genesis and geological setting. Final Proc. Int. Conf. Geological processes on Deep-Water European Margins, Moscow, Russia: UNESCO IOC Workshop Report, vol. 201, pp. 23–24.

Hein, J.R., Koski, R.A., 1987. Bacterially mediated diagenetic origin for chert-hosted manganese deposits in the Franciscan Complex, California Coast Ranges. Geology 15 (8), 722–726.

Hein, J.R., Bohrson, W.A., Schulz, M.S., Noble, M., Clague, D.A., 1992. Variations in the fine-scale composition of a central Pacific ferro-manganese crust: paleoceanographic implications. Paleoceanography 7, 63–77.

Hein, J.R., Koschinsky, A., Halbach, P., Manheim, F.T., Bau, M., Kang, J-K., Lubick, N., 1997. Iron and manganese oxide mineralization in the Pacific. Manganese Mineralization: Geochemistry and Mineralogy of Terrestrial and Marine Deposits: In: Nicholson, K., Hein, J.R., Bühn, B., Dasgupta, S. (Eds.), Special Publication Geological Society of London, London, vol. 119, pp. 123–138.

Hein, J.R. 2001. Cobalt-rich ferromanganese crusts: global distribution, composition, origin and research activities. In: ISA (Ed) Minerals other than polymetallic nodules of the International Seabed Area. Workshop Report, Kingston, Jamaica: 188–272.

Hernández-Molina, F.J., Llave, E., Somoza, L., Fernández Puga, M.C., Maestro, A., León, R., Medialdea, T., Barnolas, A., García, M., Díaz-del-Río, V., Fernández Salas, L.M., Vázquez, J.T., Lobo, F.J., Alveirinho Díaz, J.A., Rodero, J., Gardner, J., 2003. Looking for clues to paleoceanographic imprints: a diagnostic of the Gulf of Cadiz contourite depositional system. Geology 31 (1), 19–22.

Hernández-Molina, F.J., Llave, E., Stow, D.A.V., García, M., Somoza, L., Vázquez, J.T., Lobo, F.J., Maestro, A., Díaz-del-Río, V., León, R., Medialdea, T., Gardner, J., 2006. The contourite depositional system of the Gulf of Cadiz: a sedimentary model related to the bottom current activity of the Mediterranean Outflow Water and its interaction with the continental margin. Deep-Sea Research. Part 2. Topical Studies in Oceanography 53, 1420–1463.

Hinrichs, K.-U., Boetius, A., 2002. The anaerobic oxidation of methane: new insights in microbial ecology and biogeochemistry. In: Wefer, G., Billett, D., Hebbeln, D., Jørgensen, B.B., Schlüter, M., van Weering, T.C.E. (Eds.), Ocean Margin Systems. Springer-Verlag, Berlin, pp. 457–477.

Hlawatsch, S., Neumann, T., van den Berg, C.M.G., Kersten, M., Harff, J., Suess, E., 2002. Fast-growing, shallow-water ferro-manganese nodules from the western Baltic Sea: origin and modes of trace element incorporation. Marine Geology 182, 373–387.

Ingri, J. 1985. Geochemistry of ferromanganese concretions and associated sediments in the Gulf of Bothnia. PhD thesis, University of Lulea.

Ivanov, M.K., Kenyon, N., Nielsen, T., Wheeler, A., Monteiro, J., Gardner, J., Comas, M., Akhmanov, G., Akhmetzhanov, A., Scientific Party of the TTR-9 cruise, 2000. Goals and principle results of the TTR-9 cruise. Final Proc. Int. Conf. Geological processes on European Continental Margins, Granada, Spain: UNESCO IOC Workshop Report, vol. 168, pp. 24–25.

Jauhari, P., Pattan, J.N., 2000. Ferromanganese nodules from the Central Indian Ocean Basin. In: Cronan, D.S. (Ed.), Handbook of Marine Mineral Deposits. CRC Press, pp. 171–195.

Jørgensen, N.O., 1989. Holocene methane-derived, dolomite-cemented sandstone pillars from the Kattergat, Denmark. Marine Geology 88, 71–81.

Kohn, M.J., Riciputi, L.R., Stakes, D., Orange, D.L., 1998. Sulphur isotope variability in biogenic pyrite: reflections of heterogeneous bacterial colonisation? American Mineralogists 83, 1454–1468.

Koschinsky, A., Halbach, P., Hein, J.R., Mangini, A., 1996. Ferromanganese crusts as indicators for paleoceanographic events in the NE Atlantic. Geologische Rundschau 85, 567–576.

Kozlova, E., Ivanov, M., Blinova, V., 2007. The replacement of aragonite by authigenic carbonates (in the mud diapiric ridges, the Gulf of Cadiz). Geophysical Research Abstracts 9, 06912.

León, R., Somoza, L., Medialdea, T., Maestro, A., Díaz-del-Río, V., Fernández Puga, M.C., 2006. Classification of deep sea-floor features associated with methane seeps along the Gulf of Cadiz continental margin. Deep-Sea Research. Part 2. Topical Studies in Oceanography 53, 1464–1481.

León, R., Somoza, L., Medialdea, T., González, F.J., Díaz-del-Río, V., Fernández-Puga, M.C., Maestro, A., Mata, M.P., 2007. Sea-floor features related to hydrocarbon seeps in deepwater carbonate-mud mounds of the Gulf of Cadiz: from mud flows to carbonate precipitates. Geo-Marine Letters 27, 237–247.

Llave, E., Schönfeld, J., Hernández-Molina, F.J., Mulder, T., Somoza, L., Díaz-del-Río, V., Sánchez-Almazo, I., 2006. High-resolution stratigraphy of the Mediterranean outflow contourite system in the Gulf of Cadiz during the Late Pleistocene: the impact of Heinrich events. Marine Geology 227, 241–262.

Loubere, P., 1987. Changes in mid-depth North Atlantic and Mediterranean circulation during the Late Pliocene: isotope and sedimentologic evidence. Marine Geology 77, 15–38.

Lyle, M., 1981. Formation and growth of ferromanganese oxides on the Nazca plate. Nazca Plate: Crustal Formation and Andean Convergence: In: Kulm, L.D., Dymond, J., Dasch, E.J., Hussong, D.M. (Eds.), Geological Society of America Memoir, vol. 154, pp. 269–293.

Magalhães, V.H., Pinheiro, L.M., Ivanov, M., 2005. Methane-derived authigenic carbonates in the Gulf of Cadiz: cartography, distribution and controls. Eos Trans. AGU, 86 (52), Fall Meet. Suppl., Abstract OS33C-1484.

Maldonado, A., Somoza, L., Pallarés, L., 1999. The Betic Orogen and the Iberian–african boundary in the Gulf of Cadiz: geological evolution (central North Atlantic). Marine Geology 155, 9–43.
Martín-Puertas, C., Fernández-Puga, M.C., Mata, M.P., Vázquez Garrido, J.T., Díaz-del-Río, V., Somoza, L., 2006. Naturaleza de la brecha fangosa de volcanes de fango del Golfo de Cádiz: sistema diapírico del Guadalquivir y zona Tasyo. Revista de la Sociedad Geológica de España 19 (3–4), 257–270.
Martín-Puertas, C., Mata, M.P., Fernández-Puga, M.C., Díaz-del-Río, V., Vázquez, J.T., Somoza, L., 2007. A comparative mineralogical study of gas-related sediments of the Gulf of Cádiz. Geo-Marine Letters 27, 223–235.
Medialdea, T., Vegas, R., Somoza, L., Vázquez, J.T., Maldonado, A., Díaz-del-Río, V., Maestro, A., Córdoba, D., Fernández Puga, M.C., 2004. Structure and evolution of the "Olistostrome" complex of the Gibraltar Arc in the Gulf of Cadiz (eastern Central Atlantic): evidence from two long seismic cross-sections. Marine Geology 209 (1–4), 173–198.
Mottl, M.J., Wheat, C.G., Baker, E., Becker, N., Davis, E., Feely, R., Grehan, A., Kadko, D., Lilley, M., Massoth, G., Moyer, C., Sansone, F., 1998. Warm springs discovered on 3.5 Ma oceanic crust, eastern flank of the Juan de Fuca Ridge. Geology 26, 51–54.
Munsell Color Co., 1980. Munsell Soil Color Charts. Baltimore, MD.
Murray, J., Renard, A.F., 1891. Deep-sea deposits. Reports of the Scientific Results Explor. Voyage Challenger. 525 pp.
Nealson, K.H., Myers, C.R., 1992. Microbial reduction of manganese and iron: new approaches to carbon cycling. Applied and Environmental Microbiology 58–2, 439–443.
Nelson, H.C., Baraza, J., Maldonado, A., 1993. Mediterranean undercurrent sandy contourites, Gulf of Cadiz, Spain. Sedimentary Geology 82 (1–4), 103–131.
Nelson, C.H., Maldonado, A., 1999. The Cadiz Margin study off Spain: an introduction. Marine Geology 155, 3–8.
Manganese Mineralization: Geochemistry and Mineralogy of Terrestrial and Marine Deposits: Nicholson, K., Hein, J.R., Bühn, B., Dasgupta, S. (Eds.), 1997. Special Publication Geological Society of London, London, vol. 119. 370 pp.
Niemann, H., Duarte, J., Hensen, C., Omoregie, E., Magalhaes, V.H., Elvert, M., Pinheiro, L.M., Kopf, A., Boetius, A., 2006. Microbial methane turnover at mud volcanoes of the Gulf of Cadiz. Geochimica et Cosmochimica Acta 70 (21), 5336–5355.
Ochoa, J.And, Bray, N.A., 1991. Water mass exchange in the Gulf of Cadiz. Deep Sea Research 38 (1), S465–S503.
O'Neill-Barringer, M., Price, J.M., 1999. A review of physical oceanography of the Mediterranean outflow. Marine Geology 155 (1–2), 63–82.
Palma, J.J.C., Pessanha, I.B.M., 2000. Depósitos ferromanganesíferos de océano profundo. Brazilian Journal of Geophysics 18 (3), 431–446.
Peckmann, J., Reimer, A., Luth, U., Luth, C., Hansen, B.T., Heinicke, C., Hoefs, J., Reitner, J., 2001. Methane-derived carbonates and authigenic pyrite from the northwestern Black Sea. Marine Geology 177, 129–150.
Pinheiro, L.M., Ivanov, M.K., Sautkin, A., Akhmanov, G., Magalhaes, V.H., Volkonskaya, A., Monteiro, J.H., Somoza, L., Gardner, J., Hamouni, N., Cunha, M.R., 2003. Mud volcanism in the Gulf of Cadiz: results from the TTR-10 cruise. Marine Geology 195, 131–151.
Piper, D.Z., 1974. Rare earth elements in the sedimentary cycle: a summary. Chemical Geology 14, 285–305.
Raab, W.J., Meylan, M.A., 1977. Morphology. Marine Manganese Deposits: In: Glasby, G.P. (Ed.), Elsevier Oceanography Series, Amsterdam, pp. 109–146.
Reyss, J.L., Marchig, V., Ku, T.L., 1982. Rapid growth of a deep-sea manganese nodule. Nature 295, 401–403.
Robinson, B.W., Kusakabe, M., 1975. Quantitative separation of sulphur dioxide for 34S/32S analyses from sulphides by combustion with cuprous oxide. Analytical Chemistry 47, 1179–1181.
Rona, P., 2002. Marine minerals for the 21st century. Episodes 25, 2–12.
Rona, P., 2003. Resources of the sea floor. Science 299, 673–674.
Sevastýanov, V.F., Volkov, I.I., 1967. Redistribution of chemical elements in the oxidised layers of the Black Sea sediments and the formation of iron–manganese nodules. Tr. Ist. Okeanol., vol. 83, pp. 135–152.
Somoza, L., Gardner, J.M., Díaz-del-Río, V., Vázquez, J.T., Pinheiro, L., Hernández-Molina, F.J., TASYO scientific parties, 2002. Numerous methane gas-related sea floor structures identified in Gulf of Cadiz. American Geophysical Union EOS Transactions 83 (47), 541–543.
Somoza, L., Díaz-del-Río, V., León, R., Ivanov, M., Fernández-Puga, M.C., Gardner, J.M., Hernández-Molina, F.J., Pinheiro, L.M., Rodero, J., Lobato, A., Maestro, A., Vázquez, J.T., Medialdea, T., Fernández-Salas, L.M., 2003. Seabed morphology and hydrocarbon seepage in the Gulf of Cadiz mud volcano area: acoustic imagery, multibeam and ultra-high resolution seismic data. Marine Geology 195, 153–176.
Stakes, D.S., Orange, D., Paduan, J.B., Salamy, K.A., Maher, N., 1999. Cold-seeps and authigenic carbonate formation in Monterey Bay, California. Marine Geology 159, 93–109.
Stadnitskaia, A., Ivanov, M.K., Blinova, V., Kreulen, R., van Weering, T.C.E., 2006. Molecular and carbon isotopic variability of hydrocarbon gases from mud volcanoes in the Gulf of Cadiz, NE Atlantic. Marine and Petroleum Geology 23, 281–296.
Stein, L.Y., La Duc, M.T., Grundl, T.J., Nealson, K.H., 2001. Bacterial and archaeal populations associated with freshwater ferromanganese micronodules and sediments. Environmental Microbiology 3 (1), 10–18.
Verlaan, P.A., Cronan, D.S., Morgan, C.L., 2005. A comparative analysis of compositional variations in and between marine ferromanganese nodules and crusts in the South Pacific and their environmental controls. Progress in Oceanography 63, 125–158.
Volkov, I.I., 1979. Ferromanganese nodules. Oceanologiya, Khimiya Okeana, v. 2, Geokhimiya Donnykh Osadkov, pp. 414–467.
Von Stackelberg, U., 1997. Growth history of manganese nodules and crust of the Peru Basin. Manganese Mineralization: Geochemistry and Mineralogy of Terrestrial and Marine Deposits: In: Nicholson, K., Hein, J.R., Bühn, B., Dasgupta, S. (Eds.), Special Publication Geological Society of London, London, vol. 119, pp. 153–176.
Von Stackelberg, U., 2000. Manganese nodules of the Peru Basin. In: Cronan, D.S. (Ed.), Handbook of Marine Mineral Deposits. CRC Press, pp. 197–238.
Walters, L.J., Claypool, G.E., Choquette, Ph.W., 1972. Reaction rates and d 18 O variation for the carbonate-phosphoric acid preparation method. Geochimica et Cosmochimica Acta 36, 129–140.
Zhamoida, V.A., Butylin, V.P., Glasby, G.P., Popova, I.A., 1996. The nature of ferromanganese concretions from the Eastern Gulf of Finland, Baltic Sea. Marine Georesources and Geotechnology 14, 161–175.